Kaposi's sarcoma-associated herpesvirus (KSHV) utilizes the NDP52/CALCOCO2 selective autophagy receptor to disassemble processing bodies

Short title: Selective targeting of processing bodies for autophagy by KSHV

inflammatory cytokine transcripts / Kaposi's sarcoma-associated herpesvirus / NDP52 / processing bodies / selective autophagy

Carolyn-Ann Robinson[1,2,3,4,5], Gillian K. Singh[1,5], Mariel Kleer[2,3,4], Elizabeth L. Castle[1,3], Bre Q. Boudreau[1], Jennifer A. Corcoran[1,2,3,4*]

[1]Department of Microbiology & Immunology, Dalhousie University, Halifax, NS, Canada
[2]Microbiology, Immunology & Infectious Diseases Department, University of Calgary, Calgary, AB, Canada.
[3]Charbonneau Cancer Research Institute, University of Calgary, Calgary, AB, Canada.
[4]Snyder Institute for Chronic Diseases, University of Calgary, AB, Canada.
[5]Equal Contribution
[*]Corresponding Author

Abstract

Kaposi's sarcoma-associated herpesvirus (KSHV) causes the inflammatory and angiogenic endothelial cell neoplasm, Kaposi's sarcoma (KS). We previously demonstrated that expression of the KSHV protein, Kaposin B (KapB), promoted inflammation via the disassembly of cytoplasmic ribonucleoprotein granules called processing bodies (PBs). Processing bodies (PBs) modify gene expression by silencing or degrading labile messenger RNAs (mRNAs) including many transcripts that encode inflammatory or angiogenic proteins that are associated with KS disease. Although our work implicated PB disassembly as one of the causes of inflammation during KSHV infection, the precise mechanism used by KapB to elicit PB disassembly was unclear. Here we reveal a new connection between the degradative process of autophagy and PB disassembly. We show that both latent KSHV infection and KapB expression enhanced autophagic flux via the phosphorylation of the autophagy regulatory protein, Beclin 1. KapB was necessary for this effect, as infection with a recombinant virus that does not express the KapB protein did not induce Beclin 1 phosphorylation or autophagic flux. Moreover, we reveal that PB disassembly mediated by KSHV or KapB depended on canonical autophagy genes and the selective autophagy receptor *NDP52/CALCOCO2*. These studies reveal a new role for autophagy and the selective autophagy receptor NDP52 in promoting PB turnover and the concomitant synthesis of inflammatory molecules during KSHV infection.

Author Summary

Kaposi's sarcoma-associated herpesvirus (KSHV) is the causative agent of the inflammatory, endothelial cell cancer, Kaposi's Sarcoma (KS). KSHV induces a pro-tumourigenic inflammatory environment which aids in the establishment and maintenance of the KS lesion. Processing bodies (PBs) are cellular structures that dampen inflammatory gene expression by suppression or decay of their cognate RNA molecules. We previously showed that the viral protein KapB caused PB disappearance during KSHV infection, identifying a new pathway used by KSHV to elicit inflammation. Now, we show that KSHV and KapB hijack the cellular degradative process of autophagy to promote PB disassembly and increase inflammatory gene expression. This places autophagy as central to the regulation of inflammation by KSHV and illustrates another remarkable strategy used by these viruses to create a tumourigenic microenvironment.

33 **Introduction**

34 Macroautophagy, hereafter referred to as autophagy, is an evolutionarily conserved degradative
35 process that ensures the continuous recycling of material to maintain cellular homeostasis (1–3).
36 Autophagy begins with the formation of a phagophore that elongates and encloses a portion of
37 the cytoplasm to form a double-membrane organelle, the autophagosome, which fuses with
38 lysosomes to form autolysosomes, where contents are degraded (4). Under basal conditions,
39 autophagic activity ensures the clearance of damaged macromolecular complexes and organelles,
40 acting as an intracellular quality control system to maintain homeostasis (2). Various changes to
41 the cellular microenvironment, including nutrient scarcity, hypoxia, and endoplasmic reticulum
42 (ER) stress can upregulate autophagy, reprioritizing resources and promoting cell survival during
43 adverse and stressful conditions (2).

44

45 Although previously considered a non-selective bulk degradative pathway of cytoplasmic
46 recycling, recent work shows differential cargo targeting by autophagy through a process known
47 as selective autophagy (5,6). Autophagy can selectively target specific cellular components,
48 including organelles (e.g mitochondria, peroxisomes, ER) and protein complexes (e.g.
49 ribosomes, focal adhesion complexes, protein aggregates) for degradation (5,7). In selective
50 autophagy, target cargo is either selected directly, by binding to lipidated microtubule associated
51 protein 1 light chain 3 (LC3) protein (LC3-II)/Atg8, or via a receptor that mediates cargo
52 recognition. These molecular bridges are termed selective autophagy receptors (SARs), and their
53 role is to link the selected cargo to lipidated LC3-II molecules which are anchored to the
54 expanding phagophore (8). Some of the best characterized SARs include p62/SQSTM1, valosin
55 containing protein (VCP), optineurin (OPTN), neighbor of BRCA1 gene 1 (NBR1), nuclear dot

56 protein 52 (NDP52/calcium binding and coiled-coil domain protein, CALCOCO2) and its
57 paralogue TAX1BP1/CALCOCO3 (5,9,10). Of these, OPTN, p62, NDP52, and NBR1 are
58 members of the sequestosome-like family and contain several conserved motifs including a LC3-
59 interacting region (LIR) and a ubiquitin-binding domain (UBD) to mediate cargo selection via
60 binding ubiquitin chains present on the cargo surface (6,11–13).
61
62 While SARs play important homeostatic roles maintaining, and at times magnifying, the turnover
63 of organelles and aggregates via cargo selection, emerging functions of these receptors is to
64 localize the initiation of autophagy and modulate cellular signalling. SARs p62 and NDP52 both
65 promote autophagosome formation at the cargo site through direct interactions with autophagic
66 initiating complexes (14–16). SARs also play important roles in fine-tuning innate immune
67 responses by targeting key signaling platforms for degradation (17–22). For example, NDP52 is
68 required for the autophagic degradation of interferon regulatory factor 3 (IRF3) and
69 mitochondrial antiviral signaling protein (MAVS), which supports the resolution phase of type I
70 interferon signaling (19,23,24). Selective autophagy can also degrade invading pathogens such
71 as viruses in a process called xenophagy (25). Both proviral and antiviral roles have been
72 attributed to SARs (26,27) and viruses can both enhance or limit SAR function accordingly,
73 promoting their replication (28).
74
75 Kaposi's sarcoma-associated herpesvirus (KSHV) is the infectious cause of two B-cell
76 malignancies and the endothelial cell cancer, Kaposi's sarcoma (KS), which features aberrant
77 angiogenesis, tortuous leaky blood vessels, and inflammation (29–31). Infection with KSHV has
78 two forms, a latent phase and a lytic phase and it is the latent phase that predominates in KS

79 tumours (32–34). Like many viruses, KSHV manipulates the autophagic machinery. During
80 latency, the viral FLICE inhibitory protein (v-FLIP) binds Atg3 to suppress the LC3 lipidation
81 process during autophagosome biogenesis (35). KSHV also expresses a viral cyclin D homolog
82 (v-cyclin), that triggers DNA damage leading to autophagy and cellular senescence (36),
83 facilitating the production and non-conventional secretion of pro-inflammatory cytokines/
84 chemokines such as IL-1β, IL-6 and CXCL8 (37). KSHV manipulation of autophagic flux
85 prevents xenophagy, limits interferon responses, and enhances inflammatory cytokine
86 production. Precisely how KSHV fine-tunes autophagy during latency to balance proviral and
87 antiviral activities and promote inflammation and chronic viral infection is not clear.
88
89 Processing bodies (PBs) are ubiquitous, cytoplasmic, ribonucleoprotein (RNP) granules that
90 regulate expression of many cytokine RNA transcripts, making them important sites of
91 inflammatory control. PBs contain enzymes involved in mRNA turnover, including those that
92 mediate mRNA decapping (Dcp2; co-factors Dcp1a and Edc4/Hedls), 5'-3' exonucleolytic
93 degradation (5'-3' exonuclease Xrn1 and RNA helicase Rck/DDX6) and some components of
94 the RNA-induced silencing complex (28,38–43). mRNAs are routed to PBs for decay and/or
95 repression by RNA-binding proteins (RBPs) through recognition of common sequence elements
96 (39). AU-rich elements (AREs) are destabilizing RNA regulatory elements found in the 3'
97 untranslated regions (UTRs) of ~8% of cellular transcripts that are responsible for targeting
98 RNAs to PBs (44–46). When bound by destabilizing RBPs, ARE-containing RNAs are directed
99 to PBs and suppressed (47–49). Our group and others showed that PB size and numbers correlate
100 with the constitutive turnover or translational suppression of ARE-mRNAs; when PBs are
101 dispersed, this suppression is reversed (50–54). Because ARE-mRNAs encode potent regulatory

102 molecules such as inflammatory cytokines, PBs are important post-transcriptional sites of
103 regulation that fine-tune the production of inflammatory cytokines whose transcripts contain
104 AREs, including IL-6, CXCL8, IL-1β, and TNF (45,55–61).
105
106 PBs are dynamic structures that are continuously assembled and disassembled, yet relatively
107 little is known about how their activity is regulated. Stimuli that activate the p38/MK2 MAP
108 kinase pathway as well as many virus infections elicit PB disassembly and a concomitant
109 reduction in ARE-mRNA suppression to promote inflammatory molecule production
110 (50,51,54,62–64). We have previously shown that KSHV causes PB disassembly during latent
111 infection, and that the viral protein Kaposin B (KapB) induces PB disassembly while enhancing
112 the production of an ARE-containing reporter (51,62,65). These data support the notion that PB
113 disassembly is likely an important contributor to inflammation associated with KS (51,66).
114 Although we know that KapB binds and activates the kinase MK2, and that MK2 is an important
115 component of the mechanism of KapB-mediated PB disassembly and ARE-mRNA stabilization,
116 we do not precisely understand how PB loss is elicited by KapB (51,67). The observation that
117 MK2 can phosphorylate the autophagy regulatory protein Beclin 1 to increase autophagic flux in
118 response to nutrient scarcity (68) suggested to us that KapB may drive autophagic flux through
119 MK2. We now show that the KSHV KapB protein enhances autophagic flux via the
120 phosphorylation of Beclin 1, and that KSHV infection also enhances autophagic flux and Beclin
121 1 phosphorylation in a KapB-dependent manner; thus revealing an additional layer of complexity
122 in viral regulation of autophagy during KSHV latency. We show that both KSHV infection and
123 KapB alone require autophagy proteins including the selective autophagy receptor, NDP52, to
124 induce PB disassembly and that KapB requires NDP52 to elevate selected ARE-containing

125 mRNA transcripts. PB turnover is likewise elicited by the mTOR inhibitor and potent autophagy
126 inducer, Torin-1, and this process is also dependent on Atg5 and NDP52. These data forge a new
127 connection between the selective autophagy receptor NDP52 and cytoplasmic PBs and show that
128 selective autophagy of PBs is promoted by the viral protein KapB during KSHV infection.
129

130 **Results**

131 **KapB induces autophagic flux**

132 KapB expression activates the stress-responsive kinase MAPKAPK2 (MK2) (51,67). Since MK2
133 phosphorylates the essential autophagy inducer Beclin 1 in response to amino acid starvation
134 (68–70), we questioned whether KapB expression could promote autophagic flux. Essential for
135 autophagosome expansion is the lipidation of LC3 to form LC3-II, permitting its incorporation
136 into autophagosome membranes where it is degraded along with autophagosomal contents in the
137 final step of autophagy (71).. Since p62 is a selective autophagy receptor (SAR) that delivers
138 target cargo to the autophagosome, p62 is also degraded during the final step of autophagy. If
139 autophagic flux is elevated, blocking autophagic flux with a lysosomal inhibitor should result in
140 an accumulation of both p62 and LC3-II (72). To measure autophagic flux, we examined levels
141 of LC3-II and p62 with and without treatment with the lysosomal inhibitor, Bafilomycin A1
142 (BafA1). Human umbilical vein endothelial cells (HUVECs) were transduced with lentiviral
143 vectors that express KapB or an empty vector control and treated for increasing times with
144 BafA1. As expected, LC3-II and p62 accumulated in the presence of BafA1 treatment, and both
145 proteins showed higher accumulation after BafA1 treatment in KapB-expressing cells than
146 equivalently treated vector controls (Fig 1A), indicating that autophagic flux was enhanced in
147 KapB-expressing cells compared to vector controls. When KapB-expressing cells were treated
148 for 4 h with BafA1, the amount of LC3-II and p62 increased two- and four-fold, respectively
149 (Fig 1A). We also measured the formation of LC3 puncta as an indicator of autophagic flux by
150 staining KapB-expressing cells treated with BafA1 for endogenous LC3 (73,74). Untreated
151 KapB-expressing HUVECs displayed LC3 puncta area similar to that of control cells; however,

152 LC3 puncta area significantly increased after BafA1 treatment in KapB-expressing cells and not
153 in control cells, further suggesting that KapB expression enhanced autophagic flux (Fig 1B).
154
155 **KapB-mediated PB disassembly requires Atg5 and Atg14**
156 Our group previously described that MK2 activation was an important component of KapB-
157 mediated PB loss (51); however, these experiments did not reveal the precise mechanism of PB
158 loss. Since PBs are dynamic RNP granules, we wanted to determine whether KapB-mediated PB
159 loss was a result of enhanced disassembly of PBs or prevention of their *de novo* assembly. To do
160 so, we utilized HeLa cells that express a Dox-inducible GFP-tagged version of the PB-resident
161 protein, Dcp1a (41). When fixed, GFP-positive puncta co-stain with endogenous PB proteins
162 such as the RNA helicase DDX6/Rck and the decapping co-factor Hedls/Edc4, indicating that
163 they represent PBs (Fig S1). KapB was transfected into these cells either before or after inducing
164 GFP-Dcp1a granule formation. When KapB was expressed prior to granule induction, Dcp1a
165 puncta formed, although appearance of GFP-positive puncta was delayed compared to vector
166 control cells (Fig S1A). In the presence of KapB, *de novo* PB assembly was not blocked;
167 however, when KapB was expressed after PB induction, GFP-positive puncta were lost (Fig
168 S1B), indicating that KapB expression induced PB disassembly. As further evidence that KapB
169 does not prevent PB formation, we treated KapB-expressing HUVECs with sodium arsenite, a
170 known inducer of PB assembly (75). Sodium arsenite induced endogenous PB formation in
171 KapB-expressing HUVECs was indistinguishable from equivalently treated control cells (Fig
172 S1C). Taken together, these results show that KapB expression caused PB disappearance by
173 inducing PB disassembly but did not block PB assembly. We speculated that KapB may be

174 utilizing a normal cellular pathway that mediates the turnover of RNPs or their components, such
175 as autophagy.
176
177 To determine if autophagy was required for KapB-mediated PB disassembly, we first inhibited
178 autophagic flux by independently silencing two genes in the macroautophagy pathway, Atg5 and
179 Atg14 (Fig S2A, B). When either Atg5 or Atg14 were silenced in KapB-expressing HUVECs,
180 PBs were restored, whereas their silencing did not have the same effect in control cells (Fig 1C
181 and D). We then examined the ability of KapB to mediate PB disassembly in Atg5 -/- mouse
182 embryonic fibroblasts (MEFs), which (76) lack conversion of LC3-I to LC3-II (Fig S2C). KapB
183 failed to disassemble PBs in Atg5 -/- MEFs but did disassemble PBs in matched wild-type
184 controls (Fig S2D). Moreover, KapB expression resulted in a significant increase in Atg5 protein
185 levels in HUVECs (Fig S2A), consistent with our other data that show that KapB promotes
186 autophagy. Additionally, blocking autophagic degradation with BafA1 also restored PBs in
187 KapB-expressing cells (Fig 1E). Together, these data indicate that KapB mediates PB
188 disassembly by enhancing autophagy.
189
190 Autophagy, although always occurring at a basal level, can be upregulated by many different cell
191 stimuli including starvation or inhibition of mTOR using Torin-1, hereafter referred to as Torin
192 (77). It was previously reported that rapamycin, an inhibitor of mTORC1, caused a loss of PBs in
193 mammary epithelial cells (78). We reasoned that if we inhibited both mTOR complexes
194 mTORC1 and mTORC2 using Torin (79) to induce autophagy, PBs would disassemble. We
195 observed that the number of Hedls/Edc4 puncta were significantly reduced after Torin treatment,
196 indicating that chemical induction of autophagy also resulted in the disappearance of PBs (Fig

197 2A). To ensure that Torin treatment was inducing disassembly of PBs and not preventing
198 assembly, HUVECs were treated with sodium arsenite to induce PB formation; like KapB, Torin
199 treatment did not prevent the assembly of PBs under these conditions (Fig 2B).
200
201 Given these similarities, we wondered if KapB induced autophagy via inhibition of mTOR
202 complexes mTORC1 and mTORC2. To test this, we performed immunoblotting for the
203 phosphorylated form of the ribosomal protein S6 (Serine 235/236) (80) and the phosphorylated
204 form of the Unc-51 like autophagy activating kinase (ULK1; Serine 757/555), both downstream
205 targets of mTOR activation and the latter a component of the ULK autophagy initiation complex
206 (81). Unlike Torin, KapB expression did not decrease phosphorylation of S6 (Fig 2C) or ULK
207 (Fig 2D). We also tested the effect that expression of a constitutively active form of MK2 in
208 which two threonine residues that are normally phosphorylated by the upstream kinase p38, have
209 been substituted with glutamic acid residues (T205E/T317E, called MK2EE) (82–84) had on
210 phospho-S6 and phospho-ULK. We previously demonstrated that MK2EE caused PB
211 disassembly (51) and others showed it increased autophagic flux after starvation (68). Like
212 KapB, MK2EE expression did not decrease phosphorylation of S6 (Fig 2C) or ULK (Fig 2D).
213 These data indicate KapB does not inhibit mTOR activity to induce autophagy. Since KapB can
214 bind and activate MK2, we next wondered if KapB expression would mediate phosphorylation of
215 Beclin 1 at Serine 90, as shown by others for MK2EE (68). Like MK2EE, KapB induced
216 phosphorylation of Beclin 1 at Serine 90 (Fig 2E), indicating that induction of autophagy via
217 KapB expression is mediated by Beclin 1. Taken together, these data show that although both
218 KapB expression and Torin treatment caused PB disassembly in an autophagy-dependent
219 manner, the mechanism used to upregulate autophagic flux differed in each case.

220

221 **Canonical autophagy is required for KapB-mediated increases in ARE-containing cytokine**
222 **transcripts**

223 PBs are nodes of post-transcriptional mRNA regulation and microscopically visible PBs are
224 associated with ARE-mRNA decay or suppression (43,50,51,53,54,85,86). However, in
225 untreated HUVECs, the transcription of most ARE-mRNAs is minimal. To activate transcription
226 of ARE-containing cytokines in a biologically relevant manner, rather than using common
227 inflammatory stimuli such as the bacterial product, lipopolysaccharide, we treated KapB-
228 expressing or control HUVECs with 0.22 μm-filtered conditioned media from KSHV latently
229 infected cells. Conditioned media from latent KSHV cells would be expected to contain
230 inflammatory cytokines, e.g. TNF, that are elevated in KS, without containing virions (87). We
231 then examined levels of some endogenous ARE-containing RNA transcripts in KapB-expressing
232 cells (Fig 3A). We observed significant increases of cytokine mRNA for IL-6 and IL-1β in
233 KapB-expressing cells compared to equivalently treated controls, suggesting these increases
234 resulted from reduced transcript decay in PBs (Fig 3A). In addition, treatment with Torin
235 promoted the enhanced steady-state levels of IL-1β and COX-2 (Fig 3B), suggesting that
236 inducing autophagy reduced the decay of some ARE-mRNA transcripts. To support these
237 findings and to simplify further studies, we utilized a luciferase reporter assay that we developed,
238 described in (65). Using this assay, we previously showed that KapB-mediated PB loss
239 correlated with enhanced luminescence of an ARE-containing firefly luciferase (FLuc) reporter
240 because its rapid turnover was reversed and FLuc translation was enhanced (51,65). Briefly,
241 HeLa cells were co-transfected with a FLuc construct containing the destabilizing AU-rich
242 element from the *CSF2* gene in its 3'UTR and a Renilla luciferase (RLuc) construct with no

243 ARE; transcription of both reporter constructs was then stopped by the addition of doxycycline.
244 In control (vector transfected) cells, the FLuc-ARE mRNA decayed rapidly and FLuc
245 luminescence relative to the RLuc transfection control was low. Torin treatment caused a
246 significant increase in FLuc/RLuc relative luminescence compared to DMSO-treated control
247 cells, supporting our RT-qPCR findings (Fig 3C) and suggesting that enhanced autophagy
248 reverses the constitutive turnover/suppression of the ARE-mRNA reporter. Furthermore, KapB
249 expression also caused a significant increase in FLuc/RLuc relative luminescence compared to
250 empty vector control cells (Fig 3D) as previously shown in (51). When canonical autophagy was
251 perturbed by either Atg5 or Atg14 silencing (Fig S3A, B) KapB-expressing cells had
252 significantly decreased luminescence compared to KapB-expressing controls (Figs 3D, E).
253 Likewise, when KapB-expressing cells were treated with BafA1, relative luminescence was
254 significantly decreased compared to KapB-expressing untreated control cells (Fig 3F). Together,
255 these data showed that canonical autophagy is required for KapB-mediated increases in cytokine
256 mRNA levels and the enhanced expression of an ARE-mRNA reporter.
257

258 **Dcp1a protein levels are decreased by KapB and Torin treatment**

259 Both KapB and Torin mediated PB disassembly but did not prevent *de novo* PB formation. We
260 reasoned that KapB and Torin could have this effect because they cause the autophagic
261 degradation of the entire PB granule. Alternatively, since some PB proteins have important
262 scaffolding roles that hold granules together (EDC4/Hedls, Xrn1, DDX6/Rck, or Dcp1a (88)),
263 PB disassembly could be induced by KapB or Torin if one or more key PB proteins was missing
264 due to accelerated degradation. To differentiate between these two scenarios, we immunoblotted
265 for PB proteins after Torin treatment and in the context of KapB expression (Fig 4).

266 Immunoblotting revealed that steady-state levels of Dcp1a were reduced in Torin-treated (Fig
267 4A) and KapB-expressing cells (Fig 4B); however, steady-state levels of other PB-resident
268 proteins were not affected (Fig 4A, C). Moreover, KapB-mediated Dcp1a decreases were
269 reversed by BafA1 treatment (Fig 4B) and steady-state levels of the SAR, p62, included as a
270 measure of autophagic flux, were likewise restored (Fig 4B). Together, these data suggest that
271 autophagy induction with Torin or KapB expression promote the accelerated degradation of the
272 PB-resident protein Dcp1a, but not all PB proteins. Silencing the canonical autophagy gene,
273 *Atg5*, resulted in a reversal of KapB-mediated Dcp1a loss (Fig 4D), suggesting that autophagy is
274 required for the loss of Dcp1a observed in KapB-expressing cells.
275
276 **KapB-mediated PB disassembly and ARE-mRNA stabilization require the selective**
277 **autophagy receptor NDP52**
278 After establishing a link between KapB expression, autophagy, and PB disassembly, we
279 wondered what specific autophagy mechanisms were at work and if selective autophagy
280 receptors (SARs) were involved. One previous study observed the SAR, NDP52, partially co-
281 localized with some PB proteins (89). For this reason, we used RNA silencing to investigate
282 whether NDP52, p62, VCP, NBR1, or OPTN were required for KapB-mediated PB disassembly.
283 Despite trying several different shRNA sequences, our attempts to silence NBR1 were
284 unsuccessful, and shRNAs targeting VCP resulted in significant HUVEC toxicity (Fig S4A, B).
285 Therefore, the role of these molecules in KapB-mediated PB disassembly could not be
286 determined. Knockdown of NDP52, p62, and OPTN was validated in control and KapB-
287 expressing cells (Fig S4C-E). Silencing of p62 or OPTN did not restore PBs in KapB-expressing
288 cells whereas NDP52 knockdown significantly restored PBs (Fig 5A, Fig S4F). These data

289 pinpointed an important role for NDP52 and selective autophagy in KapB-mediated PB
290 disassembly. We then tested whether NDP52 silencing could prevent Torin-mediated PB
291 disassembly and found that PBs could not be disassembled in cells lacking NDP52 (Fig 5B,
292 S4G). We also examined whether these SARs were required for KapB-enhanced relative
293 luminescence in our ARE-mRNA reporter assay. We validated silencing of NDP52, p62, and
294 OPTN in HeLa cells (Fig S5A-C). Similarly, we found that p62 or OPTN knockdown had no
295 effect on KapB-mediated ARE-containing reporter luminescence, but NDP52 silencing
296 decreased the signal compared to non-targeting, KapB-expressing controls (Fig 5C), further
297 supporting the role of NDP52 in autophagy-mediated PB disassembly. We then performed an
298 NDP52 complementation experiment. We first silenced endogenous NDP52 in control or KapB-
299 expressing HUVECs using shRNAs targeting the 3'UTR of NDP52 and verified its knockdown
300 (Fig S6A). Next, NDP52 expression was restored by overexpressing a fluorescently tagged
301 NDP52 construct. Complementation of NDP52-silenced HUVECs with NDP52 restored KapB-
302 mediated PB disassembly compared to vector controls (Fig 5D-E; S6B, C). Taken together, these
303 data indicate that NDP52 is required for KapB- and Torin-mediated PB disassembly and KapB-
304 mediated ARE-mRNA stabilization.
305
306 **Atg5 and NDP52 are required for KSHV-mediated PB disassembly**
307 Autophagy regulation during KSHV latency is complex, as the viral gene products v-FLIP and v-
308 cyclin also modulate autophagic flux in addition to KapB (35,36). To simplify our study of
309 autophagy and PBs, we initially used a reductionist approach, expressing only KapB in
310 HUVECs. However, to confirm the relevance of our study to KSHV infection, we performed a
311 study in KSHV-infected HUVECs. We infected cells with rKSHV.219 (90) for 96 hours to

312 permit latency establishment and then treated or with either BafA1 or a vehicle control for 30
313 minutes prior to staining infected cells for LC3 puncta as a measure of autophagic flux. We
314 observed a dramatic increase in LC3 puncta in KSHV infected cells after BafA1 treatment when
315 compared to mock infection controls (Fig 6A). These data demonstrate that autophagic flux was
316 upregulated during KSHV latency despite the concurrent expression of vFLIP, an inhibitor of
317 autophagy, during this infection phase.(35). In parallel, we immunoblotted infected cell lysates
318 and observed that KSHV increased phosphorylation of Ser90 of Beclin 1 (Fig 6B), consistent
319 with earlier observations of Ser90 phosphorylation after ectopic expression of KapB (Fig 2D).
320 To confirm if KapB was necessary for upregulated autophagic flux after KSHV infection, we
321 used a recombinant KSHV that does not express KapB (delB BAC16) and matched wild-type
322 control (BAC16 KSHV), described in our recent publication (91). Primary infection of HUVECs
323 with BAC16 KSHV also induced LC3 puncta formation and phosphorylation of Ser90 of Beclin
324 1, consistent with our result using the KSHV.219 virus, whereas infection with delB BAC16
325 virus failed to enhance autophagic flux or phosphorylation of Beclin 1 at Ser90 (Fig 6C, D).
326 Together, these data validate a necessary role for KapB in KSHV enhancement of autophagic
327 flux and show that during this KSHV infection phase, autophagy proceeds via a non-canonical
328 activation mechanism that involves phosphorylation of Ser90 in Beclin 1 (68).
329
330 In our previous work, we showed that KSHV infection induced PB disassembly (51) and more
331 recently we confirmed that KapB was not only sufficient but also necessary for this effect with
332 the delB BAC16 virus (91) . To determine if autophagic machinery is also required for PB
333 disassembly in the context of KSHV infection, we silenced *Atg5* or *NDP52* in HUVECs prior to
334 infecting with rKSHV.219 for 96 hours, then stained for PBs. Consistent with our data that

335 showed a requirement for autophagy in KapB-mediated PB disassembly , blocking autophagic
336 degradation with silencing *Atg5* or *NDP52* restored PBs in KSHV-infected cells (Fig 7A). We
337 quantified PBs and compared their levels between KSHV-infected and mock-infected cells in
338 control cells or in silenced cells. We did not compare PB counts between KSHV-infected and
339 silenced cells to infected controls because silencing of autophagy regulatory proteins influences
340 PB homeostasis. In control cells that expressed a non-targeting shRNA, KSHV infection
341 decreased PBs, as expected from our previous work (Fig 7B). However, when either *Atg5* or
342 *NDP52* were silenced, KSHV infection had no effect on PBs relative to the matched uninfected
343 control, and silencing autophagy regulatory proteins restored PBs to levels observed in the
344 absence of infection (Fig 7B). These data confirm an essential role for autophagy and the
345 selective autophagy receptor NDP52 in KSHV-mediated PB disassembly.
346

347 **Discussion**

348 Here, we demonstrated that the KSHV protein KapB relies on selective autophagy to cause PB
349 disassembly and enhance ARE-mRNA stability. Furthermore, we identified NDP52 as the
350 selective autophagy receptor required for this process. To our knowledge, this is the first report
351 that NDP52 regulates the turnover of endogenous PBs and the first description of the
352 contribution of NDP52 to immune regulation by altering inflammatory cytokine RNA
353 turnover/suppression in PBs. We also showed that PB disassembly induced by infection with
354 KSHV required Atg5 and NDP52, suggesting an important role for KapB-mediated elevated
355 autophagic flux and PB catabolism in regulating KSHV-associated inflammation. Our major
356 findings are: i) KapB and KSHV latent infection increased autophagic flux by phosphorylation
357 of the autophagy regulatory protein, Beclin 1, thereby contributing to the complex regulation of
358 autophagic processes during KSHV latent infection and tumourigenesis, ii) KapB expression was
359 necessary for KSHV-mediated autophagy increases, iii) KapB- and KSHV-mediated PB
360 disassembly and enhanced translation of an ARE-containing reporter required canonical
361 autophagy machinery and the selective autophagy receptor, NDP52, iv) Activation of autophagy
362 by chemical inhibition of mTORC1 using Torin caused PB disassembly using a mechanism that
363 was dependent on canonical autophagy and NDP52, suggesting that KapB manipulates an
364 existing cellular pathway that regulates PB catabolism. These results reveal that PB turnover
365 elicited by the KSHV KapB protein during infection requires a host pathway that uses NDP52 to
366 enhance PB catabolism and promote inflammatory molecule production.

367

368 MK2 activation promotes autophagy by phosphorylating Beclin 1 (68); therefore, we
369 hypothesized that KapB, an MK2-activating viral protein (67), would utilize autophagy to

370 promote PB clearance. Our data showed that both KapB and MK2EE increased autophagic flux
371 via phosphorylation of Beclin 1 at Serine 90 and that KapB-mediated PB disassembly required
372 the canonical autophagy proteins Atg5 and Atg14, and the selective autophagy protein NDP52.
373 Our data are supported by previous work showing that in yeast, PB recycling requires canonical
374 autophagy machinery, and in mammalian cells NDP52 colocalizes with a GFP-tagged version of
375 Dcp1a when overexpressed (89,92). We add significantly to these studies, by performing our
376 work in primary human endothelial cells and by staining for endogenous PBs using
377 immunofluorescence for the decapping co-factor Hedls/EDC4. We revealed that when KapB was
378 expressed, endogenous PBs disassemble via an Atg5-, Atg14-, and NDP52-dependent
379 mechanism. We also complemented NDP52-silenced cells with an shRNA-resistant NDP52 and
380 observed the restoration of KapB-mediated PB disassembly. These data suggest that it is the
381 ability of NDP52 to bind cargo for autophagic degradation that is required for KSHV and KapB-
382 mediated PB disassembly, as has been observed in other studies on NDP52 SAR function
383 (93,94). In addition to identifying cargo for clearance, NDP52 has recently been shown to
384 orchestrate autophagosome biogenesis by recruiting essential autophagic machinery to initiation
385 sites (14,95,96), suggesting another possible way that NDP52 may promote KapB-mediated PB
386 disassembly.
387
388 Immunoelectron microscopy showed that PBs range in size from 150 to 350 nm and possess an
389 external area of peripheral protrusions that contain the helicase Rck/DDX6 anchored to a dense
390 central core of decay enzymes, including Dcp1a and Xrn1 (38). Many PB-localized enzymes are
391 required for PB stability including Dcp1a; however, only three PB proteins are required for *de*
392 *novo* PB formation, DDX6, the translation suppressor, 4E-T, and LSM14a (88). Our data showed

393 that KapB expression decreased the steady-state levels of Dcp1a, while the steady-state levels of
394 other PB proteins were unaffected. Inducing autophagy with the mTORC1/2 inhibitor Torin
395 recapitulated this effect, decreasing steady-state levels of Dcp1a, but not other PB proteins.
396 These data support a model where the entire PB granule is not degraded by autophagy, but PB
397 disassembly is induced by the selective degradation of Dcp1a or another unidentified PB protein.
398 Consistent with this, we show that PBs can still form during KapB expression if we overexpress
399 Dcp1a-GFP or block translation using sodium arsenite. Dcp1a is also a target for other viruses
400 that mediate PB disassembly; for example, infection with poliovirus also caused PB disassembly
401 and the loss of Dcp1a over a time course of infection (97). We do not yet understand how KapB
402 expression or Torin treatment alters Dcp1a to promote its degradation and the resultant PB
403 disassembly, but we speculate that modulation of known post-translational modifications of
404 Dcp1a, such as phosphorylation or ubiquitination, may be involved (98–104). In our model, we
405 propose that KapB expression increases the recognition of Dcp1a or another PB protein by
406 NDP52, which then targets the protein to nascent autophagosomes (Fig 7C).
407
408 Infection with KSHV induces high levels of pro-inflammatory cytokines, chemokines and
409 angiogenic factors such as TNF, IL-1α, IL-1β, IL-6, CXCL8, IFN-γ, VEGF, COX-2 and GM-CSF
410 (55–61). Although several KSHV proteins promote the transcription of these products, many harbor
411 AREs in the 3'UTR of their cognate mRNA, meaning their transcripts are subject to additional post-
412 transcriptional regulation by PBs. We previously showed that KapB and the lytic KSHV protein,
413 viral G-protein-coupled receptor (vGPCR) enhanced the translation of an ARE-containing reporter
414 and elevated steady-state levels of inflammatory products, and that this coincided with the ability of
415 KapB and vGPCR to induce PB disassembly (50,51,65,67). We now show that KapB expression
416 increased steady-state levels of three ARE-containing transcripts, IL-6, GM-CSF, and TNF,

417 coincident with PB disassembly. However, KapB expression did not increase CXCL8, indicating
418 that there remains additional regulation, beyond PB disassembly, of ARE-mRNA decay
419 (105,106). We also show that the ability of KapB to induce PB disassembly and enhance our ARE-
420 mRNA reporter requires both canonical and selective autophagic machinery. RNA transcripts for
421 some canonical autophagy proteins in the Atg5-Atg12-Atg16 complex are also rendered labile by
422 3'UTR AREs, suggesting that expression of KapB or vGPCR may cause a pro-autophagic
423 positive feedback loop where PB disassembly culminates in the enhanced translation of pro-
424 autophagic products (107,108), a feature that may be aided further by KapB-mediated
425 upregulation of the ARE-mRNA stabilizing RBP, HuR (109). This feed forward loop may
426 contribute to the KapB-mediated increase in Atg5 protein levels and the induction of autophagic
427 flux. Taken together, our study reveals a novel way that KSHV infection manipulates autophagic
428 machinery to induce PB turnover and promote inflammatory molecule production. The fact that
429 KSHV encodes more than one protein that reverses the constitutive repression of inflammatory
430 mRNAs in PBs highlights its central importance.
431
432 Viral gene products both enhance and block autophagic flux during latent KSHV infection; v-
433 cyclin induces oncogene-induced senescence via induction of autophagy, whereas v-FLIP
434 counteracts v-cyclin, blocking autophagy by binding Atg3 and inhibiting LC3 lipidation (35,36).
435 We show herein that KapB also upregulates autophagic flux, and that KapB is necessary for the
436 enhanced autophagic flux we observe after KSHV infection of ECs. These data are consistent
437 with autophagy enhancement observed in latent B-lymphocytes (110) and show for the first time
438 that KSHV infection of primary ECs culminates in an elevated autophagic state. It is possible
439 that KSHV products may cooperate to promote autophagy during latency, perhaps via
440 dysregulation of the cellular transcription factor, Nrf2, responsible for the activation of several

441 antioxidant response genes as well as NDP52 (111–113). Nrf2 activity is upregulated by the viral
442 protein vFLIP after *de novo* infection of ECs and during KSHV latency (114,115). Thus, despite
443 being an established negative regulator of autophagic flux, vFLIP may indirectly promote the
444 selective autophagy of PBs during KSHV latency by increasing NDP52 expression, thereby
445 synergizing with KapB-mediated effects on autophagy.
446
447 In viral cancers like KS, autophagic flux promotes a pro-tumourigenic and pro-inflammatory
448 environment (110,116–118). The data shown herein brings new understanding to this complex
449 relationship during KSHV infection. We show that KapB was both sufficient to induce
450 autophagic flux and was necessary for enhanced autophagy after primary KSHV infection. We
451 confirmed that autophagy machinery and NDP52 were required for PB disassembly; this
452 supports an important role for KapB in eliciting the pro-inflammatory environment associated
453 with latent KSHV infection and KS. The manipulation of NDP52 function and autophagic flux
454 by KSHV and KapB is yet another example of the ingenuity with which viruses usurp cellular
455 processes; revealing a regulatory network that links NDP52 to inflammatory molecule
456 production via PB catabolism.
457

458 **Materials and Methods**

459 **Cell culture**

460 All cells were grown at 37 °C with 5% CO_2 and 20% O_2. HEK293T cells (ATCC), HeLa Tet-Off
461 cells (Clontech), Atg5 +/+ and -/- MEFs (119), HeLa Flp-In TREx GFP-Dcp1a cells (a generous
462 gift from Anne-Claude Gingras), and iSLK.219 cells (a generous gift from Don Ganem) (90)
463 were cultured in DMEM (Thermo Fisher) supplemented with 100 U/mL penicillin, 100 µg/mL
464 streptomycin, 2 mM L-glutamine (Thermo Fisher) and 10% FBS (Thermo Fisher). iSLK.219
465 cells were additionally cultured in the presence of puromycin (10 µg/mL). HUVECs (Lonza)
466 were cultured in endothelial cell growth medium (EGM-2) (Lonza). HUVECs were seeded onto
467 gelatin (1% w/v in PBS)-coated tissue culture plates or glass coverslips. All drug treatments were
468 performed for the times indicated in each experiment at the concentrations listed in Table 1.

469 **Cloning**

470 All plasmids used in this study can be found in Table 2. All shRNAs were generated by cloning
471 shRNA hairpin sequences found in Table 3 into pLKO.1-TRC Puro (pLKO.1-TRC cloning
472 vector was a gift from David Root (Addgene plasmid # 10878; http://n2t.net/addgene:10878;
473 RRID:Addgene_10878) or pLKO.1-blast (pLKO.1-blast was a gift from Keith Mostov (Addgene
474 plasmid #26655; http://n2t.net/addgene:26655; RRID:Addgene_26655).

475 **Lentivirus Production and Transduction**

476 All lentiviruses were generated using a second-generation system. Briefly, HEK293T cells were
477 transfected with pSPAX2, MD2G, and the plasmid containing a gene of interest or hairpin using
478 polyethylimine (PEI, Polysciences). psPAX2 was a gift from Didier Trono (Addgene plasmid
479 #12260; http://n2t.net/addgene:12260; RRID:Addgene_12260) and pMD2.G was a gift from
480 Didier Trono (Addgene plasmid #12259; http://n2t.net/addgene:12259; RRID:Addgene_12259).

481

482 Viral supernatants were harvested 48 h post-transfection, clarified using a 0.45 μ
483 polyethersulfone filter (VWR), and frozen at -80°C until use. For transduction, lentiviruses were
484 thawed at 37°C and added to target cells in complete media containing 5 μg/mL polybrene
485 (Sigma) for 24 h. The media was changed to selection media containing 1 μg/mL puromycin or 5
486 μg/mL blasticidin (Thermo) and cells were selected for 48 h before proceeding with
487 experiments.

488 **Viral conditioned media treatments**

489 iSLK.219 cells (latently infected with rKSHV.219 virus) were sub-cultured into a 10 cm cell
490 culture dish and grown without puromycin for 72 h. At 72 h, conditioned media was reserved
491 and cleared of cellular debris by centrifugation at 500 G for 5 min. Supernatant was collected
492 and filtered through a 0.22 μM polyethersulfone (PES) membrane filter (VWR) and stored in
493 aliquots at -80. Prior to the experiment, conditioned media was thawed at 37°C and combined
494 1:1 with fresh HUVEC EGM-2 media and used to treat vector or KapB-expressing HUVECs for
495 0 or 6 h prior to total RNA harvest.

496 **Production of KSHV**

497 Cloning and creation of the iSLK-BAC16ΔKapB cell line is described in (91). iSLK.219 or
498 iSLK-BAC16 cells were sub-cultured into a 10 cm cell culture dish without puromycin and
499 reactivated from latency with either 1 μg/mL doxycycline (Sigma-Aldrich) alone (iSLK.219) and
500 1 μg/mL doxycycline and 1 mM sodium butyrate (Sigma-Aldrich) (iSLK-BAC16). After 72 h,
501 supernatants were collected, centrifuged to remove cellular debris, aliquoted, and stored at -80°C
502 until use.

503 ***De novo* infection of HUVECs**

504 Sub-confluent (50-70%) 12-well plates of HUVECs were incubated with either rKSHV.219 or
505 KSHV BAC16 viral inoculum diluted in antibiotic and serum free DMEM containing 5 µg/mL
506 polybrene. Plates were centrifuged at 800 x *g* for 2 hours at room temperature (120), the
507 inoculum was removed and replaced with either EGM-2. For KSHV BAC16 infections, WT and
508 ΔKapB inoculums were normalized empirically prior to infection to circumvent our previously
509 observed impairment in latency establishment during ΔKapB infection (91).

510 **Immunofluorescence**

511 Cells were seeded onto coverslips for immunofluorescence experiments and fixed for 10 mins at
512 37 °C in 4% (v/v) paraformaldehyde (Electron Microscopy Sciences). Samples were
513 permeabilized with 0.1% (v/v) Triton X-100 (Sigma-Aldrich) for 10 min at room temperature
514 and blocked in 1% human AB serum (Sigma-Aldrich) for 1 h at room temperature. For
515 autophagosome immunofluorescence cells were fixed for 10 min in ice cold methanol at -20 °C
516 and blocked in 1% human AB serum for 1 h at room temperature. Primary and secondary
517 antibodies were diluted in 1% human AB serum and used at the concentrations in Table 4.
518 Samples were mounted with Prolong Gold AntiFade mounting media (Thermo). Image analysis
519 was performed using CellProfiler (cellprofiler.org), an open source platform for image analysis
520 (Carpenter et al., 2006); quantification of puncta was performed as previously described, with the
521 exception that cells were defined by propagating out a set number of pixels from each nucleus
522 (121).

523 **Immunoblotting**

524 Cells were lysed in 2x Laemmli buffer and stored at -20°C until use. The DC Protein Assay
525 (Bio-Rad) was used to quantify protein concentration as per the manufacturer's instructions. 10-
526 15 µg of protein lysate was resolved by SDS-PAGE on TGX Stain-Free acrylamide gels

527 (BioRad). Total protein images were acquired from the PVDF membranes after transfer on the
528 ChemiDoc Touch Imaging system (BioRad). Membranes were blocked in 5% bovine serum
529 albumin (BSA) or skim milk in Tris-buffered saline-Tween20 (TBS-T). Primary and secondary
530 antibodies were diluted in 2.5% BSA or skim milk, dilutions can be found in Table 4.
531 Membranes were visualized using Clarity Western ECL substrate and the ChemiDoc Touch
532 Imaging system (BioRad).

533 **Luciferase Assays**

534 Luciferase assays were performed as previously described (65). HeLa Tet-Off cells were
535 transduced with recombinant lentivirus expressing different shRNAs and selected. Cells were
536 transfected according to Corcoran *et al.* (2011) with pTRE2 Firefly Luciferase ARE (FLuc),
537 pTRE2 Renilla Luciferase (RLuc), and the expression plasmid of interest using Fugene HD
538 (Promega). FLuc and RLuc activity were quantified using the Dual Luciferase Assay Kit
539 (Promega) and read on a GloMax multi-detection system (Promega).

540 **Quantitative PCR**

541 RNA was collected using a RNeasy Plus Mini Kit (Qiagen) according to the manufacturer's
542 instructions and stored at -80°C until further use. RNA concentration was determined and was
543 reverse transcribed using Maxima H Minus First Strand cDNA Synthesis Kit (Thermo Fisher)
544 using a combination of random and oligo (dT) primers according to the manufacturer's
545 instructions. cDNA was diluted either 1:5 or 1:10 for all qPCR experiments and GoTaq qPCR
546 Master Mix (Promega) was used to amplify cDNA. The ΔΔquantitation cycle (Cq) method was
547 used to determine the fold change in expression of target transcripts. qPCR primer sequences can
548 be found in Table 5.

549 **Statistics**

550 Data shown are the mean ± standard error of the mean (SEM). Statistical significance was
551 determined using a one-way ANOVA, a 2-way ANOVA or Student's t-test when appropriate
552 with the applicable post-test (indicated in the corresponding figure legends). All statistics were
553 performed using GraphPad Prism v.9.0.
554

555 **Acknowledgements**

556 The authors would like to dedicate this manuscript to Dr. Beth Levine, who was a leader in the
557 field of autophagy and viruses and who inspired this work. We sincerely thank the members of
558 the Corcoran lab for helpful discussions about this work. We would like to thank Dr. Craig
559 McCormick (Dalhousie University), Dr. Eric Pringle (Dalhousie University), and Dr. Andrew
560 Leidal (UCSF) for valuable feedback on this manuscript and the McCormick lab for plasmids,
561 expertise, and advice. We would like to thank Mr. Stephen Whitefield and Ms. Mary Ann
562 Trevors in the Dalhousie *CORES* (Cellular and Molecular Digital Imaging and Electron
563 Microscopy core facilities) and Dr. Anne Vaahtokari of the Charbonneau Microscopy Facility,
564 UCalgary for microscopy support. We would like to thank Dr. Andreas Till (University of
565 Bonn), Dr. Anne-Claude Gingras (Lunenfeld-Tanenbaum Research Institute) and Dr. Don
566 Ganem (Novartis) for sharing valuable reagents. Model figure created with BioRender. GKS was
567 supported by a CIHR CGS-M scholarship and Scotia Scholars NSHRF graduate training award.
568 ELC was supported by a Killam predoctoral scholarship, an NSERC CGS-M scholarship, and a
569 Nova Scotia Graduate scholarship. MK was supported by a CSM graduate training award, a
570 CIHR CGS-M scholarship, and a CIHR doctoral award. Operating funds to support this work
571 derive from a CIHR Project Grant PJT-153210 to JAC.
572

Author Contributions

Carolyn-Ann Robinson: Conceptualization, Experimentation, Analysis, Paper Writing

Gillian K. Singh: Conceptualization, Experimentation, Analysis, Paper Writing

Mariel Kleer: Experimentation, Analysis, Paper Writing

Elizabeth L. Castle: Analysis

Bre Q. Boudreau: Experimentation

Jennifer A. Corcoran: Conceptualization, Experimentation, Supervision, Funding Acquisition, Project Administration, Paper Writing

Conflict of Interest

The authors have no competing interests to declare.

586 **References**
587
588 1. Dikic I, Elazar Z. Mechanism and medical implications of mammalian autophagy. Nat
589 Rev Mol Cell Biol. 2018;19:349–64.
590 2. Levine B, Kroemer G. Biological Functions of Autophagy Genes: A Disease Perspective.
591 Cell. 2019;176: 11-42.
592 3. Morishita H, Mizushima N. Diverse cellular roles of autophagy. Annu Rev Cell Dev Biol.
593 2019;35: 453–75.
594 4. Lawrence RE, Zoncu R. The lysosome as a cellular centre for signalling, metabolism and
595 quality control. Nat Cell Biol. 2019;21:133-142.
596 5. Beese CJ, Brynjólfsdóttir SH, Frankel LB. Selective Autophagy of the Protein
597 Homeostasis Machinery: Ribophagy, Proteaphagy and ER-Phagy. Front Cell Dev Biol.
598 2020;7: 373.
599 6. Johansen T, Lamark T. Selective Autophagy: ATG8 Family Proteins, LIR Motifs and
600 Cargo Receptors. J Mol Biol. 2020;432: 80-103.
601 7. Kirkin V, Rogov V V. A Diversity of Selective Autophagy Receptors Determines the
602 Specificity of the Autophagy Pathway. Mol Cell. 2019;76: 268-285.
603 8. Rogov V, Dötsch V, Johansen T, Kirkin V. Interactions between Autophagy Receptors
604 and Ubiquitin-like Proteins Form the Molecular Basis for Selective Autophagy. Mol Cell.
605 2014;53:167–78.
606 9. Tumbarello DA, Manna PT, Allen M, Bycroft M, Arden SD, Kendrick-Jones J, et al. The
607 Autophagy Receptor TAX1BP1 and the Molecular Motor Myosin VI Are Required for
608 Clearance of Salmonella Typhimurium by Autophagy. PLoS Pathog. 2015;11: e1005174.
609 10. Sarraf SA, Shah H V., Kanfer G, Pickrell AM, Holtzclaw LA, Ward ME, et al. Loss of

610 TAX1BP1-Directed Autophagy Results in Protein Aggregate Accumulation in the Brain.
611 Mol Cell. 2020;80: 779-785.
612 11. Khaminets A, Behl C, Dikic I. Ubiquitin-Dependent And Independent Signals In Selective
613 Autophagy. Trends Cell Biol. 2016;26: 6–16.
614 12. Rogov V V, Stolz A, Ravichandran AC, Rios-Szwed DO, Suzuki H, Kniss A, et al.
615 Structural and functional analysis of the GABARAP interaction motif (GIM). EMBO Rep.
616 2017;18: 1382-1396.
617 13. Marshall RS, Hua Z, Mali S, McLoughlin F, Vierstra RD. ATG8-Binding UIM Proteins
618 Define a New Class of Autophagy Adaptors and Receptors. Cell. 2019;177: 766-781.
619 14. Ravenhill BJ, Boyle KB, von Muhlinen N, Ellison CJ, Masson GR, Otten EG, et al. The
620 Cargo Receptor NDP52 Initiates Selective Autophagy by Recruiting the ULK Complex to
621 Cytosol-Invading Bacteria. Mol Cell. 2019;74: 320-329
622 15. Turco E, Witt M, Abert C, Bock-Bierbaum T, Su MY, Trapannone R, et al. How
623 RB1CC1/FIP200 claws its way to autophagic engulfment of SQSTM1/p62-ubiquitin
624 condensates. Autophagy. 2019;15: 1475-77.
625 16. Vargas JNS, Wang C, Bunker E, Hao L, Maric D, Schiavo G, et al. Spatiotemporal
626 Control of ULK1 Activation by NDP52 and TBK1 during Selective Autophagy. Mol Cell.
627 2019;74: 347-362.
628 17. Chen M, Meng Q, Qin Y, Liang P, Tan P, He L, et al. TRIM14 Inhibits cGAS
629 Degradation Mediated by Selective Autophagy Receptor p62 to Promote Innate Immune
630 Responses. Mol Cell. 2016;64(1):105–19.
631 18. Du Y, Duan T, Feng Y, Liu Q, Lin M, Cui J, et al. LRRC25 inhibits type I IFN signaling
632 by targeting ISG15-associated RIG-I for autophagic degradation. EMBO J.

633 2018;37(3):351–66.
634 19. Jin S, Tian S, Luo M, Xie W, Liu T, Duan T, et al. Tetherin Suppresses Type I Interferon
635 Signaling by Targeting MAVS for NDP52-Mediated Selective Autophagic Degradation in
636 Human Cells. Mol Cell. 2017;68:308-322.
637 20. Prabakaran T, Bodda C, Krapp C, Zhang B, Christensen MH, Sun C, et al. Attenuation of
638 c GAS - STING signaling is mediated by a p62/ SQSTM 1-dependent autophagy pathway
639 activated by TBK1. EMBO J. 2018;37: e97858.
640 21. Yang Q, Liu TT, Lin H, Zhang M, Wei J, Luo WW, et al. TRIM32-TAX1BP1-dependent
641 selective autophagic degradation of TRIF negatively regulates TLR3/4-mediated innate
642 immune responses. PLoS Pathog. 2017;13: e1006600.
643 22. He X, Zhu Y, Zhang Y, Geng Y, Gong J, Geng J, et al. RNF 34 functions in immunity
644 and selective mitophagy by targeting MAVS for autophagic degradation. EMBO J.
645 2019;38: e100978.
646 23. Seth RB, Sun L, Ea CK, Chen ZJ. Identification and characterization of MAVS, a
647 mitochondrial antiviral signaling protein that activates NF-κB and IRF3. Cell.
648 2005;122:669–82.
649 24. Wu Y, Jin S, Liu Q, Zhang Y, Ma L, Zhao Z, et al. Selective autophagy controls the
650 stability of transcription factor IRF3 to balance type I interferon production and immune
651 suppression. Autophagy. 2020;17: 1376-92
652 25. Orvedahl A, Levine B. Viral evasion of autophagy. Autophagy. 2008;4: 280–5.
653 26. Sumpter R, Levine B. Selective autophagy and viruses. Autophagy. 2011;7: 260–5.
654 27. Ahmad L, Mostowy S, Sancho-Shimizu V. Autophagy-virus interplay: From cell biology
655 to human disease. Front Cell Dev Biol. 2018;6: 155.

656 28. Mohamud Y, Qu J, Xue YC, Liu H, Deng H, Luo H. CALCOCO2/NDP52 and
657 SQSTM1/p62 differentially regulate coxsackievirus B3 propagation. Cell Death Differ.
658 2019;26: 1062–76.
659 29. Cesarman E, Chang Y, Moore PS, Said JW, Knowles DM. Kaposi's sarcoma-associated
660 herpesvirus-like DNA sequences in AIDS-related body-cavity-based lymphomas. N Engl
661 J Med. 1995;332: 1186–91.
662 30. Chang Y, Cesarman E, Pessin MS, Lee F, Culpepper J, Knowles DM, et al. Identification
663 of herpesvirus-like DNA sequences in AIDS-associated Kaposi's sarcoma. Science.
664 1994;266: 1865–9.
665 31. Soulier J, Grollet L, Oksenhendler E, Cacoub P, Cazals-Hatem D, Babinet P, et al.
666 Kaposi's sarcoma-associated herpesvirus-like DNA sequences in multicentric Castleman's
667 disease. Blood. 1995;86: 1276–80.
668 32. Decker LL, Shankar P, Khan G, Freeman RB, Dezube BJ, Lieberman J, et al. The Kaposi
669 sarcoma-associated herpesvirus (KSHV) is present as an intact latent genome in KS tissue
670 but replicates in the peripheral blood mononuclear cells of KS patients. J Exp Med.
671 1996;184: 283–8.
672 33. Staskus KA, Zhong W, Gebhard K, Herndier B, Wang H, Renne R, et al. Kaposi's
673 sarcoma-associated herpesvirus gene expression in endothelial (spindle) tumor cells. J
674 Virol. 1997;71: 715–9.
675 34. Broussard G, Damania B. Regulation of KSHV Latency and Lytic Reactivation. Viruses.
676 MDPI AG; 2020;12: 1034.
677 35. Lee J-S, Li Q, Lee J-Y, Lee S-H, Jeong JH, Lee H-R, et al. FLIP-mediated autophagy
678 regulation in cell death control. Nat Cell Biol. 2009;11: 1355–62.

679 36. Leidal AM, Cyr DP, Hill RJ, Lee PWK, McCormick C. Subversion of autophagy by
680 Kaposi's sarcoma-associated herpesvirus impairs oncogene-induced senescence. Cell
681 Host Microbe. 2012;11: 167–80.
682 37. Young ARJ, Narita M, Ferreira M, Kirschner K, Sadaie M, Darot JFJ, et al. Autophagy
683 mediates the mitotic senescence transition. Genes Dev. 2009;23: 798–803.
684 38. Cougot N, Cavalier A, Thomas D, Gillet R. The Dual Organization of P-bodies Revealed
685 by Immunoelectron Microscopy and Electron Tomography. J Mol Biol. 2012;420: 17–28.
686 39. Hubstenberger A, Courel M, Bénard M, Souquere S, Ernoult-Lange M, Chouaib R, et al.
687 P-Body Purification Reveals the Condensation of Repressed mRNA Regulons. Mol Cell.
688 2017;68:144-157.
689 40. Corbet GA, Parker R. RNP granule formation: Lessons from P-bodies and stress granules.
690 Cold Spring Harb Symp Quant Biol. 2019;84: 203–15.
691 41. Youn JY, Dunham WH, Hong SJ, Knight JDR, Bashkurov M, Chen GI, et al. High-
692 Density Proximity Mapping Reveals the Subcellular Organization of mRNA-Associated
693 Granules and Bodies. Mol Cell. 2018;69: 517-532.
694 42. Riggs CL, Kedersha N, Ivanov P, Anderson P. Mammalian stress granules and P bodies at
695 a glance. J Cell Sci. 2020;133: jcs242487 .
696 43. Luo Y, Na Z, Slavoff SA. P-Bodies: Composition, Properties, and Functions.
697 Biochemistry. 2018;57: 2424.
698 44. Barreau C, Paillard L, Osborne HB. AU-rich elements and associated factors: Are there
699 unifying principles? Nucleic Acids Res. Oxford University Press; 2005;33: 7138–50.
700 45. Bakheet T, Hitti E, Khabar KSA. ARED-Plus: An updated and expanded database of AU-
701 rich element-containing mRNAs and pre-mRNAs. Nucleic Acids Res. 2018;46:D218–20.

702 46. García-Mauriño SM, Rivero-Rodríguez F, Velázquez-Cruz A, Hernández-Vellisca M,
703 Díaz-Quintana A, De la Rosa MA, et al. RNA binding protein regulation and cross-talk in
704 the control of AU-rich mRNA Fate. Front Mol Biosci. 2017;4: 71.
705 47. Maitra S, Chou CF, Luber CA, Lee KY, Mann M, Chen CY. The AU-rich element mRNA
706 decay-promoting activity of BRF1 is regulated by mitogen-activated protein kinase-
707 activated protein kinase 2. RNA. 2008;14: 950–9.
708 48. Lai WS, Carballo E, Strum JR, Kennington EA, Phillips RS, Blackshear PJ. Evidence that
709 Tristetraprolin Binds to AU-Rich Elements and Promotes the Deadenylation and
710 Destabilization of Tumor Necrosis Factor Alpha mRNA. Mol Cell Biol. 1999;19: 4311–
711 23.
712 49. Lai WS, Blackshear PJ. Interactions of CCCH zinc finger proteins with mRNA.
713 Tristetraprolin-mediated AU-rich element-dependent mRNA degradation can occur in the
714 absence of a poly(A) tail. J Biol Chem. 2001;276: 23144–54.
715 50. Corcoran JA, Khaperskyy DA, Johnston BP, King CA, Cyr DP, Olsthoorn A V., et al.
716 Kaposi's Sarcoma-Associated Herpesvirus G-Protein-Coupled Receptor Prevents AU-
717 Rich-Element-Mediated mRNA Decay. J Virol. 2012;86:8859–71.
718 51. Corcoran JA, Johnston BP, McCormick C. Viral activation of MK2-hsp27-p115RhoGEF-
719 RhoA signaling axis causes cytoskeletal rearrangements, p-body disruption and ARE-
720 mRNA stabilization. PLoS Pathog. 2015;11:e1004597.
721 52. Franks TM, Lykke-Andersen J. TTP and BRF proteins nucleate processing body
722 formation to silence mRNAs with AU-rich elements. Genes Dev. 2007;21: 719–35.
723 53. Blanco FF, Sanduja S, Deane NG, Blackshear PJ, Dixon D a. Transforming growth factor
724 β regulates P-body formation through induction of the mRNA decay factor tristetraprolin.

725 Mol Cell Biol. 2014;34: 180–95.

726 54. Vindry C, Marnef A, Broomhead H, Twyffels L, Ozgur S, Stoecklin G, et al. Dual RNA
727 Processing Roles of Pat1b via Cytoplasmic Lsm1-7 and Nuclear Lsm2-8 Complexes. Cell
728 Rep. 2017;20:1187–200.

729 55. Ensoli B, Nakamura S, Salahuddin SZ, Biberfeld P, Larsson L, Beaver B, et al. AIDS-
730 Kaposi's Sarcoma-Derived Cells Express Cytokines with Autocrine and Paracrine Growth
731 Effects. Science. 2010;243:223–6.

732 56. Ensoli B, Stürzl M. Kaposi's sarcoma: a result of the interplay among inflammatory
733 cytokines, angiogenic factors and viral agents. Cytokine Growth Factor Rev. 1998;9: 63–
734 83.

735 57. Lane BR, Liu J, Bock PJ, Schols D, Coffey MJ, Strieter RM, et al. Interleukin-8 and
736 growth-regulated oncogene alpha mediate angiogenesis in Kaposi's sarcoma. J Virol.
737 2002;76: 11570–83.

738 58. Miles SA, Rezai AR, Salazar-González JF, Vander Meyden M, Stevens RH, Logan DM,
739 et al. AIDS Kaposi sarcoma-derived cells produce and respond to interleukin 6. Proc Natl
740 Acad Sci U S A. 1990;87: 4068–72.

741 59. Riva G, Barozzi P, Torelli G, Luppi M. Immunological and Inflammatory Features of
742 Kaposi's Sarcom and Other Kaposi's Sarcoma-Associated Herpesvirus/Human
743 Herpesvirus 8-Associated Neoplasias. AIDS Rev. 2010;9: 25–39.

744 60. Sadagopan S, Sharma-Walia N, Veettil MV, Raghu H, Sivakumar R, Bottero V, et al.
745 Kaposi's Sarcoma-Associated Herpesvirus Induces Sustained NF-κB Activation during
746 De Novo Infection of Primary Human Dermal Microvascular Endothelial Cells That Is
747 Essential for Viral Gene Expression. J Virol. 2007;8: 3949–68.

748 61. Salahuddin S, Nakamura S, Biberfeld P, Kaplan M, Markham P, Larsson L, et al.
749 Angiogenic properties of Kaposi's sarcoma-derived cells after long-term culture in vitro.
750 Science. 1988;242:430–3.
751 62. Corcoran JA, McCormick C. Viral activation of stress-regulated Rho-GTPase signaling
752 pathway disrupts sites of mRNA degradation to influence cellular gene expression. Small
753 GTPases. 2015;6: 178–85.
754 63. Standart N, Weil D. P-Bodies: Cytosolic Droplets for Coordinated mRNA Storage. Trends
755 Genet. 2018;34: 612–26.
756 64. Docena G, Rovedatti L, Kruidenier L, Fanning Á, Leakey NAB, Knowles CH, et al.
757 Down-regulation of p38 mitogen-activated protein kinase activation and proinflammatory
758 cytokine production by mitogen-activated protein kinase inhibitors in inflammatory bowel
759 disease. Clin Exp Immunol. 2010;162: 108–15.
760 65. Corcoran JA, Khaperskyy DA, McCormick C. Assays for monitoring viral manipulation
761 of host ARE-mRNA turnover. Methods. 2011;55: 172–81.
762 66. Wen KW, Damania B. Kaposi sarcoma-associated herpesvirus (KSHV): molecular
763 biology and oncogenesis. Cancer Lett. 2010;289: 140–50.
764 67. McCormick C, Ganem D. The Kaposin B Protein of KSHV Activates the p38/MK2
765 Pathway and Stabilizes Cytokine mRNAs. Science. 2005;307: 739–41.
766 68. Wei Y, An Z, Zou Z, Sumpter R, Su M, Zang X, et al. The stress-responsive kinases
767 MAPKAPK2/MAPKAPK3 activate starvation-induced autophagy through Beclin 1
768 phosphorylation. Elife. 2015;4: e05289.
769 69. Shen L, Qi Z, Zhu Y, Song X, Xuan C, Ben P, et al. Phosphorylated heat shock protein 27
770 promotes lipid clearance in hepatic cells through interacting with STAT3 and activating

771 autophagy. Cell Signal. 2016;28: 1086–98.

772 70. Gurkar AU, Chu K, Raj L, Bouley R, Lee S-H, Kim Y-B, et al. Identification of ROCK1
773 kinase as a critical regulator of Beclin1-mediated autophagy during metabolic stress. Nat
774 Commun. 2013;4: 2189.

775 71. Klionsky DJ, Abdel-Aziz AK, Abdelfatah S, Abdellatif M, Abdoli A, Abel S, et al.
776 Guidelines for the use and interpretation of assays for monitoring autophagy (4th edition).
777 Autophagy. 2021;17: 1-382.

778 72. Mizushima N, Murphy LO. Autophagy Assays for Biological Discovery and Therapeutic
779 Development. Trends Biochem Sci. 2020;45: 1080-1093.

780 73. Mizushima N, Yoshimori T, Levine B. Methods in Mammalian Autophagy Research.
781 Cell. 2010;140: 313–26.

782 74. Mauvezin C, Neufeld TP. Bafilomycin A1 disrupts autophagic flux by inhibiting both V-
783 ATPase-dependent acidification and Ca-P60A/SERCA-dependent autophagosome-
784 lysosome fusion. Autophagy. 2015;11:1437–8.

785 75. Kedersha N, Anderson P. Mammalian Stress Granules and Processing Bodies. Meth
786 Enzymol. 2007;431: 61-81.

787 76. Katayama H, Yamamoto A, Mizushima N, Yoshimori T, Miyawaki A. GFP-like proteins
788 stably accumulate in lysosomes. Cell Struct Funct. 2008;33: 1–12.

789 77. Thoreen CC, Kang SA, Won Chang J, Liu Q, Zhang J, Gao Y, et al. An ATP-competitive
790 Mammalian Target of Rapamycin Inhibitor Reveals Rapamycin-resistant Functions of
791 mTORC1. J Biol Chem. 2009;284: 8023–32.

792 78. Hardy SD, Shinde A, Wang W-H, Wendt MK, Geahlen RL. Regulation of epithelial-
793 mesenchymal transition and metastasis by TGF-β, P-bodies, and autophagy. Oncotarget.

794 2017;8: 103302–14.
795 79. Liu Q, Xu C, Kirubakaran S, Zhang X, Hur W, Liu Y, et al. Characterization of Torin2, an
796 ATP-competitive inhibitor of mTOR, ATM, and ATR. Cancer Res. 2013;73: 2574–86.
797 80. Kuang E, Tang Q, Maul GG, Zhu F. Activation of p90 Ribosomal S6 Kinase by ORF45 of
798 Kaposi's Sarcoma-Associated Herpesvirus and Its Role in Viral Lytic Replication. J Virol.
799 2008;82: 1838-50.
800 81. Kim J, Kundu M, Viollet B, Guan KL. AMPK and mTOR regulate autophagy through
801 direct phosphorylation of Ulk1. Nat Cell Biol. 2011;13: 132-41.
802 82. Kayyali US, Pennella CM, Trujillo C, Villa O, Gaestel M, Hassoun PM. Cytoskeletal
803 changes in hypoxic pulmonary endothelial cells are dependent on MAPK-activated protein
804 kinase MK2. J Biol Chem. 2002;277: 42596–602.
805 83. Rousseau S, Houle F, Landry J, Huot J. P38 MAP kinase activation by vascular
806 endothelial growth factor mediates actin reorganization and cell migration in human
807 endothelial cells. Oncogene [Internet]. 1997 [cited 2021 Jan 28];15(18):2169–77.
808 Available from: https://pubmed.ncbi.nlm.nih.gov/9393975/
809 84. Engel K, Schultz H, Martin F, Kotlyarov A, Plath K, Hahn M, et al. Constitutive
810 activation of mitogen-activated protein kinase-activated protein kinase 2 by mutation of
811 phosphorylation sites and an A-helix motif. J Biol Chem. 1995;270: 27213–21.
812 85. Guo L, Louis IV-S, Bohjanen PR. Post-transcriptional regulation of cytokine expression
813 and signaling. Curr Trends Immunol. 2018;19: 33–40.
814 86. Franks TM, Lykke-Andersen J. The control of mRNA decapping and P-body formation.
815 Mol Cell. 2008;32: 605–15.
816 87. Sharma-Walia N, Paul AG, Bottero V, Sadagopan S, Veettil MV, Kerur N, et al. Kaposi's

817 Sarcoma Associated Herpes Virus (KSHV) induced COX-2: A key factor in latency,
818 inflammation, angiogenesis, cell survival and invasion. PLoS Pathog. 2010;6: e1000777.
819 88. Ayache J, Bénard M, Ernoult-Lange M, Minshall N, Standart N, Kress M, et al. P-body
820 assembly requires DDX6 repression complexes rather than decay or Ataxin2/2L
821 complexes. Mol Biol Cell. 2015;26: 2579–95.
822 89. Guo H, Chitiprolu M, Gagnon D, Meng L, Perez-Iratxeta C, Lagace D, et al. Autophagy
823 supports genomic stability by degrading retrotransposon RNA. Nat Commun. 2014;5:
824 5276.
825 90. Myoung J, Ganem D. iSLK cell. J Virol Methods. 2011;174: 12–21.
826 91. Kleer M, MacNeil G, Adam N, Pringle ES, Corcoran JA. A panel of KSHV mutants in the
827 polycistronic kaposin locus for precise analysis of individual protein products. J Virol.
828 2021; JVI015621. Online ahead of print.
829 92. Buchan JR, Kolaitis R, Taylor JP, Parker R. Eukaryotic Stress Granules Are Cleared by
830 Autophagy and Cdc48 / VCP Function. Cell. 2013;153: 1461–74.
831 93. Xie X, Li F, Wang Y, Wang Y, Lin Z, Cheng X, et al. Molecular basis of ubiquitin
832 recognition by the autophagy receptor CALCOCO2. Autophagy. 2015;11: 1775–89.
833 94. Cemma M, Kim PK, Brumell JH. The ubiquitin-binding adaptor proteins p62/SQSTM1
834 and NDP52 are recruited independently to bacteria-associated microdomains to target
835 Salmonella to the autophagy pathway. Autophagy. 2011;7: 341–5.
836 95. Yamano K, Youle RJ. Two different axes CALCOCO2-RB1CC1 and OPTN-ATG9A
837 initiate PRKN-mediated mitophagy. Autophagy. 2020;16: 2105–7.
838 96. Shi X, Chang C, Yokom AL, Jensen LE, Hurley JH. The autophagy adaptor ndp52 and the
839 fip200 coiled-coil allosterically activate ulk1 complex membrane recruitment. Elife.

840 2020;9: 1–20.
841 97. Dougherty JD, White JP, Lloyd RE. Poliovirus-mediated disruption of cytoplasmic
842 processing bodies. J Virol. 2011;85: 64–75.
843 98. Bish R, Cuevas-Polo N, Cheng Z, Hambardzumyan D, Munschauer M, Landthaler M, et
844 al. Comprehensive Protein Interactome Analysis of a Key RNA Helicase: Detection of
845 Novel Stress Granule Proteins. Biomolecules. 2015;5: 1441–66.
846 99. Gustafson EA, Wessel GM. DEAD-box helicases: posttranslational regulation and
847 function. Biochem Biophys Res Commun. 2010;395: 1–6.
848 100. Rahman H, Qasim M, Oellerich M, Asif AR. Crosstalk between Edc4 and mammalian
849 target of rapamycin complex 1 (mTORC1) signaling in mRNA decapping. Int J Mol Sci.
850 2014;15: 23179–95.
851 101. Yoon J-H, Choi E-J, Parker R. Dcp2 phosphorylation by Ste20 modulates stress granule
852 assembly and mRNA decay in Saccharomyces cerevisiae. J Cell Biol. 2010;189: 813–27.
853 102. Tenekeci U, Poppe M, Beuerlein K, Busch J, Schmitz ML, Kracht Correspondence M.
854 K63-Ubiquitylation and TRAF6 Pathways Regulate Mammalian P-Body Formation and
855 mRNA Decapping. Mol Cell. 2016;62: 943–57.
856 103. Aizer A, Kafri P, Kalo A, Shav-Tal Y. The P Body Protein Dcp1a Is Hyper-
857 phosphorylated during Mitosis. Prigent C, editor. PLoS One. 2013;8: e49783.
858 104. Chiang PY, Shen YF, Su YL, Kao CH, Lin NY, Hsu PH, et al. Phosphorylation of mRNA
859 Decapping Protein Dcp1a by the ERK Signaling Pathway during Early Differentiation of
860 3T3-L1 Preadipocytes. PLoS One. 2013;8: e61697.
861 105. Palanisamy V, Park NJ, Wang J, Wong DT. AUF1 and HuR proteins stabilize interleukin-
862 8 mRNA in human saliva. J Dent Res. 2008;87: 772–6.

863 106. Palanisamy V, Jakymiw A, Van Tubergen EA, D'Silva NJ, Kirkwood KL. Control of
864 Cytokine mRNA Expression by RNA-binding Proteins and microRNAs. J Dent Res.
865 2012;91: 651–8.
866 107. Lystad AH, Carlsson SR, de la Ballina LR, Kauffman KJ, Nag S, Yoshimori T, et al.
867 Distinct functions of ATG16L1 isoforms in membrane binding and LC3B lipidation in
868 autophagy-related processes. Nat Cell Biol. 2019;21: 372–83.
869 108. Ji E, Kim C, Kang H, Ahn S, Jung M, Hong Y, et al. RNA Binding Protein HuR Promotes
870 Autophagosome Formation by Regulating Expression of Autophagy-Related Proteins 5,
871 12, and 16 in Human Hepatocellular Carcinoma Cells. Mol Cell Biol. 2019;39: e00508-
872 18.
873 109. Yoo J, Kang J, Lee HN, Aguilar B, Kafka D, Lee S, et al. Kaposin-B enhances the
874 PROX1 mRNA stability during lymphatic reprogramming of vascular endothelial cells by
875 Kaposi's sarcoma herpes virus. PLoS Pathog. 2010;6: e1001046.
876 110. Pringle ES, Robinson C-A, McCormick C. Kaposi's Sarcoma-Associated Herpesvirus
877 Lytic Replication Interferes with mTORC1 Regulation of Autophagy and Viral Protein
878 Synthesis. J Virol. 2019;93: e00854-19.
879 111. Jo C, Gundemir S, Pritchard S, Jin YN, Rahman I, Johnson GVW. Nrf2 reduces levels of
880 phosphorylated tau protein by inducing autophagy adaptor protein NDP52. Nat Commun.
881 2014;5: 3496.
882 112. Moi P, Chan K, Asunis I, Cao A, Kan YW. Isolation of NF-E2-related factor 2 (Nrf2), a
883 NF-E2-like basic leucine zipper transcriptional activator that binds to the tandem NF-
884 E2/AP1 repeat of the β-globin locus control region. Proc Natl Acad Sci U S A. 1994;91:
885 9926–30.

886 113. Nguyen T, Nioi P, Pickett CB. The Nrf2-antioxidant response element signaling pathway
887 and its activation by oxidative stress. J Biol Chem. 2009;284: 13291–5.
888 114. Gjyshi O, Bottero V, Veettil MV, Dutta S, Singh VV, Chikoti L, et al. Kaposi's sarcoma-
889 associated herpesvirus induces Nrf2 during de novo infection of endothelial cells to create
890 a microenvironment conducive to infection. PLoS Pathog. 2014;10: e1004460.
891 115. Gjyshi O, Flaherty S, Veettil MV, Johnson KE, Chandran B, Bottero V. Kaposi's
892 Sarcoma-Associated Herpesvirus Induces Nrf2 Activation in Latently Infected Endothelial
893 Cells through SQSTM1 Phosphorylation and Interaction with Polyubiquitinated Keap1. J
894 Virol. 2015;89: 2268–86.
895 116. Vescovo T, Pagni B, Piacentini M, Fimia GM, Antonioli M. Regulation of Autophagy in
896 Cells Infected With Oncogenic Human Viruses and Its Impact on Cancer Development.
897 Front Cell Dev Biol. 2020;8: 47.
898 117. Liu J, Debnath J. The Evolving, Multifaceted Roles of Autophagy in Cancer. Adv Cancer
899 Res. 2016;130: 1–53.
900 118. Wu WKK, Coffelt SB, Cho CH, Wang XJ, Lee CW, Chan FKL, et al. The autophagic
901 paradox in cancer therapy. Oncogene. 2012;31: 939–53.
902 119. Kuma A, Hatano M, Matsui M, Yamamoto A, Nakaya H, Yoshimori T, et al. The role of
903 autophagy during the early neonatal starvation period. Nature. 2004;432: 1032–6.
904 120. Yoo SM, Ahn AK, Seo T, Hong HB, Chung MA, Jung SD, et al. Centrifugal enhancement
905 of Kaposi's sarcoma-associated virus infection of human endothelial cells in vitro. J Virol
906 Methods. 2008;154: 160-6.
907 121. Castle EL, Robinson C-A, Douglas P, Rinker KD, Corcoran JA. Viral manipulation of a
908 mechanoresponsive signaling axis disassembles processing bodies. Mol Cell Biol.

909 2021;41: e0039921.

910 122. Moffat J, Grueneberg DA, Yang X, Kim SY, Kloepfer AM, Hinkle G, et al. A Lentiviral
911 RNAi Library for Human and Mouse Genes Applied to an Arrayed Viral High-Content
912 Screen. Cell. 2006;124: 1283–98.

913 123. Bryant DM, Datta A, Rodríguez-Fraticelli AE, PeräCurrency Signnen J, Martín-Belmonte
914 F, Mostov KE. A molecular network for de novo generation of the apical surface and
915 lumen. Nat Cell Biol. 2010;12: 1035–45.

916 124. Johnston BP, Pringle ES, McCormick C. KSHV activates unfolded protein response
917 sensors but suppresses downstream transcriptional responses to support lytic replication.
918 PLoS Pathog. 2019;15: e1008185.

919
920

921 **Figure Legends**

922 **Figure 1: Kaposin B requires canonical autophagy to disassemble PBs.** Primary human
923 umbilical vein endothelial cells (HUVECs) were transduced with recombinant lentiviruses
924 expressing either Kaposin B (KapB) or an empty vector control and selected with blasticidin (5
925 µg/mL). A: Cells were treated with Bafilomycin A1 (BafA1, 10 nM) or a vehicle control
926 (DMSO) for the indicated times prior to harvest in 2x Laemmli buffer. Protein lysates were
927 resolved by SDS-PAGE and immunoblot was performed for p62 and LC3. Samples were
928 quantified using Image Lab (Biorad) software and then normalized, first to total protein and then
929 to their respective starting time points (0 h). Results were plotted in GraphPad and a linear
930 regression statistical test was performed, ±SEM; n=3, *=P<0.05, ***=P<0.001. B: Cells were
931 treated with BafA1 for 30 min prior to fixation in methanol. Immunofluorescence was performed
932 for LC3 (white) and DAPI (nuclei, blue). Scale bar=20 µm. Total LC3 area per field was
933 quantified by identifying LC3-positive puncta using CellProfiler and normalizing to the number
934 of nuclei and the vector DMSO control. Results were plotted in GraphPad, a 2-way ANOVA was
935 performed with a Šidák's multiple comparison test, matched data from each replicate was paired
936 for comparison, ±SEM; n=3, *=P<0.05. C, D: HUVECs were sequentially transduced: first with
937 recombinant lentiviruses expressing either shRNAs targeting Atg5 (C) or Atg14 (D) (shAtg5,
938 shAtg14) or a non-targeting control (NS) and selected with puromycin (1 µg/mL), and second
939 with either KapB or an empty vector control and selected with blasticidin (5 µg/mL). Coverslips
940 were fixed in 4% paraformaldehyde, permeabilized in 0.1% Triton X-100, and immunostained
941 for the PB-resident protein Hedls (white) and nuclei (DAPI). Scale bar=20 µm. Hedls puncta
942 were quantified using CellProfiler and presented as number of Hedls puncta per cell, all cells
943 counted are displayed. Results were plotted in GraphPad and a 2-way ANOVA was performed

944 on the main column effects with a Tukey's multiple comparison test, bar represents the mean;
945 n=4 (C), n=3 (D), ****=P<0.0001. E: HUVECs were treated as in B. Coverslips were fixed in
946 4% paraformaldehyde, permeabilized in 0.1% Triton X-100, and immunostained for the PB-
947 resident protein Hedls (white) and nuclei (DAPI). Scale bar=20 µm. Hedls puncta were
948 quantified using CellProfiler and presented as number of Hedls puncta per cell, all cells counted
949 are displayed. Results were plotted in GraphPad and a 2-way ANOVA was performed on the
950 main column effects with a Tukey's multiple comparison test, bar represents the mean; n=3,
951 **=P<0.01.
952
953 **Figure 2: Torin treatment disassembles PBs.** A: HUVECs were treated with either Torin (250
954 nM) or a DMSO control for 2 h prior to fixation in 4% paraformaldehyde. Samples were
955 permeabilized in 0.1% Triton X-100. Immunofluorescence was performed for Hedls (PBs, white)
956 and DAPI (nuclei, blue). Scale bar=20 µm. Hedls puncta were quantified using CellProfiler and
957 presented as number of Hedls puncta per cell, all cells counted are displayed. Results were
958 plotted in GraphPad and a 2-way ANOVA was performed on the main column effects with a
959 Tukey's multiple comparison test, bar represents the mean; n=3, ****=P<0.0001. B: HUVECs
960 were treated with either Torin (250 nM) or a DMSO control for 90 min prior to the addition of
961 sodium arsenite (0.25 mM) for 30 min. Cells were fixed in 4% paraformaldehyde and
962 permeabilized in 0.1% Triton X-100. Immunofluorescence was performed for Hedls (PBs, white)
963 and DAPI (nuclei, blue). Scale bar=20 µm. C: HUVECs were transduced with recombinant
964 lentiviruses expressing either KapB, constitutively active MK2 (MK2EE), or an empty vector
965 control and selected with blasticidin (5 µg/mL). Cells were treated with either Torin (250 nM) or
966 a DMSO control for 2 h prior to harvest in 2x Laemmli buffer. Protein lysates were resolved by

967 SDS-PAGE and immunoblot was performed for phospho-S6 (Ser235/236) and total S6. D:
968 HUVECs were transduced and treated as in C and harvested in 2X Laemmli buffer. Protein
969 lysates were resolved by SDS-PAGE and immunoblot was performed for phospho-ULK
970 (Ser757), phospho-ULK (Ser555), and total ULK. E: HUVECs were transduced as in C and
971 harvested in 2X Laemmli buffer. Protein lysates were resolved by SDS-PAGE and immunoblot
972 was performed for phospho-Beclin 1 (Ser90) and total Beclin 1. Samples were quantified by
973 normalizing total and phospho-Beclin 1 protein levels to the total protein in each lane and then
974 using Image Lab (Biorad), normalizing to the Vector control, and then dividing phospho- over
975 total Beclin 1. Results were plotted in GraphPad and a one-way ANOVA was performed with a
976 Dunnett's test, ±SEM; n=4, *=P<0.05.
977
978 **Figure 3: KapB-mediated ARE-mRNA reporter expression requires canonical autophagy.**
979 A: HUVECs were transduced with recombinant lentiviruses expressing either KapB or an empty
980 vector control and selected with blasticidin (5 µg/mL). Conditioned media harvested from
981 r.219.KSHV latently infected iSLK cells was used to mimic the KS lesion microenvironment
982 and induce the transcription of cytokines for 6 h prior to lysis for total RNA, normal media was
983 used for the 0 h time point. Transcript levels were quantified by qPCR and normalized to 18S as
984 a reference gene. Data is represented as the fold change in target transcript expression relative to
985 the untreated vector control and was quantified using the ΔΔCq method. Results were plotted in
986 GraphPad, a 2-way ANOVA was performed, ±SEM; n=3, *=P<0.05, **=P<0.01. B: HUVECs
987 were treated with Torin (250 nM) or a DMSO control for 2 h prior to lysis for total RNA.
988 Transcript levels were quantified by qPCR and normalized to HPRT as a reference gene. Data is
989 represented as the fold change in target transcript expression relative to the untreated vector

990 control and was quantified using the ΔΔCq method. An unpaired t-test was performed, ±SEM;
991 n=3, *=P<0.05. C: HeLa Tet-Off cells were co-transfected with expression plasmids for an ARE-
992 containing firefly luciferase plasmid (pTRE-FLuc-ARE) and a stable renilla luciferase plasmid
993 (pTRE-RLuc). 36 h post transfection, doxycycline (Dox) was added to halt reporter gene
994 transcription of both luciferase reporters, at the same time Torin (250 nM) or DMSO were added;
995 12 h after Dox addition, lysates were harvested in passive lysis buffer (Promega). Luciferase
996 activity for both FLuc and RLuc was analyzed using the Dual-Luciferase Reporter Assay
997 (Promega) and normalized (FLuc/RLuc) relative luciferase was calculated in relative light units
998 (RLUs). Results were plotted using GraphPad, an unpaired t-test was performed, ±SEM; n=6,
999 ***=P<0.001. D&E: HeLa Tet-Off cells were transduced with recombinant lentiviruses
1000 expressing either shRNAs targeting Atg5 or Atg14 (shAtg5, shAtg14) or a non-targeting control
1001 (NS) and selected with puromycin (1 µg/mL). After selection, cells were co-transfected and Dox
1002 treatment was performed as described in C, except that co-transfection also included an
1003 expression plasmid for KapB or an empty vector control. Results were plotted using GraphPad,
1004 an unpaired t-test was performed, ±SEM; n=3, *=P<0.05, **=P<0.01. F: Cells were co-
1005 transfected as in E and BafA1 (10 nM) was added at the same time as Dox. Results were plotted
1006 in GraphPad and a Student's t-test was performed, ±SEM; n=3, *=P<0.05, **=P<0.01.
1007
1008 **Figure 4: Dcp1a protein levels are decreased by KapB expression and Torin treatment.** A:
1009 HUVECs were treated with DMSO or Torin (250 nM) for 4 h prior to harvest. Samples were
1010 lysed in 2x Laemmli buffer and resolved by SDS-PAGE before immunoblotting with Xrn1,
1011 EDC4/Hedls, Dcp1a, and DDX6. Samples were quantified by normalizing the PB resident
1012 protein levels to the total protein in each lane and then the DMSO control using ImageLab

1013 (Biorad). Results were plotted in GraphPad and a one-way ANOVA was performed ±SEM; n=3,
1014 **=P<0.01. B: HUVECs were transduced with recombinant lentiviruses expressing either KapB
1015 or an empty vector control and selected with blasticidin (5 µg/mL). Cells were treated with
1016 DMSO or bafilomycin A1 (BafA1, 10 nM) for 4 h prior to harvest in 2x Laemmli buffer.
1017 Samples were resolved by SDS-PAGE and immunoblot was performed for Dcp1a or p62
1018 (autophagy marker). Samples were quantified by normalizing Dcp1a protein levels to the total
1019 protein in each lane using Image Lab (Biorad) and then to the Vector DMSO control. Results
1020 were plotted in GraphPad and a 2-way ANOVA was performed, ±SEM; n=3, ***=P<0.001. C:
1021 HUVECs were transduced with recombinant lentiviruses expressing either KapB or an empty
1022 vector control and selected with blasticidin (5 µg/mL). Samples were harvested in 2x Laemmli
1023 buffer, resolved by SDS-PAGE and immunoblot was performed for Xrn1, Hedls/EDC4, or
1024 DDX6. Samples were quantified by normalizing PB protein levels to the total protein in each
1025 lane using Image Lab (Biorad) and then to the Vector control. Results were plotted in GraphPad.
1026 D: HUVECs were sequentially transduced: first with recombinant lentiviruses expressing either
1027 shRNAs targeting Atg5 (shAtg5) or a non-targeting control (NS) and selected with puromycin (1
1028 µg/mL), and second with either KapB or an empty vector control and selected with blasticidin (5
1029 µg/mL). Samples were harvested in 2x Laemmli buffer and resolved by SDS-PAGE.
1030 Immunoblot was performed for Dcp1a, Atg5, and KapB. Samples were quantified by
1031 normalizing Dcp1a protein levels to the total protein in each lane using Image Lab (Biorad) and
1032 then to the Vector NS control. Results were plotted in GraphPad and a 2-way ANOVA was
1033 performed, ±SEM; n=3, *=P<0.05, **P=<0.01.
1034

1035 **Figure 5: KapB-mediated PB disassembly and ARE-mRNA reporter expression require the**
1036 **selective autophagy receptor NDP52**. A: HUVECs were sequentially transduced with
1037 recombinant lentivirus expressing KapB or an empty vector control and selected with blasticidin
1038 (5 µg/mL), and second with shRNAs targeting NDP52 or a non-targeting control (NS) and
1039 selected with puromycin (1 µg/mL). Coverslips were fixed in 4% paraformaldehyde,
1040 permeabilized in 0.1% Triton X-100 and immunostained for Hedls (PBs; white), DAPI (nuclei,
1041 blue). Scale bar=20 µm. Hedls puncta were quantified using CellProfiler and presented as
1042 number of Hedls puncta per cell, all cells counted are displayed. Results were plotted in
1043 GraphPad and a 2-way ANOVA was performed on the main column effects with a Tukey's
1044 multiple comparison test, bar represents the mean; n=3, *=P<0.05. B: HUVECs were transduced
1045 with recombinant lentivirus expressing an shRNA targeting NDP52 and selected with puromycin
1046 (1 µg/mL). Cells were treated with Torin (250 nM) or a DMSO control for 2 h prior to fixation in
1047 4% paraformaldehyde and permeabilization in 0.1% Triton X-100. Samples were immunostained
1048 for Hedls (PBs; white), DAPI (nuclei, blue). Scale bar=20 µm. Hedls puncta were quantified
1049 using CellProfiler and presented as number of Hedls puncta per cell, all cells counted are
1050 displayed. Results were plotted in GraphPad and a 2-way ANOVA was performed on the main
1051 column effects with a Tukey's multiple comparison test, bar represents the mean; n=3,
1052 ****=P<0.0001. C: HeLa Tet-Off cells were transduced with recombinant lentivirus expressing
1053 shRNAs targeting NDP52, OPTN, p62 or a NS control and selected with puromycin (1µg/mL)
1054 then cells were co-transfected, treated with Dox and luciferase activity was recorded and
1055 analyzed as in Figure 3. Data were plotted in GraphPad as the mean fold change in the relative
1056 luciferase activity of each condition compared to vector NS or KapB NS; n=4. An unpaired t-test
1057 was performed; * = P<0.05 **= P<0.01. D: HUVECs were sequentially transduced first with

1058 recombinant lentivirus expressing shDNP52 targeting the 3'-UTR of NDP52 or a NS control and
1059 selected with blasticidin (5 µg/mL), and second, with KapB and either mCherry control (mCh) or
1060 RFP-NDP52. Coverslips were fixed with 4% paraformaldehyde, permeabilized with 0.1% Triton
1061 X-100, and immunostained with Hedls (PBs, green). Scale bar=20 µm. E: Samples from D were
1062 quantified; Hedls puncta were quantified using CellProfiler and presented as number of Hedls
1063 puncta per cell, all cells counted are displayed. Results were plotted in GraphPad and a 2-way
1064 ANOVA was performed on the main column effects with a Tukey's multiple comparison test,
1065 bar represents the mean; n=3, ****=P<0.0001.
1066
1067 **Figure 6: KSHV infection induces autophagic flux and phosphorylation of Beclin 1.** A:
1068 HUVECs were infected with rKSHV.219 via spinoculation and infection was allowed to proceed
1069 for 96 h prior to treatment with bafilomycin A1 (10 nM) for 30 min. Coverslips were fixed in
1070 methanol and immunostained for LC3 (autophagosomes; white) and DAPI (nuclei, blue). Cells
1071 were visually assessed for infection via LANA immunofluorescence. Scale bar=20 µm. Total
1072 LC3 area per field was quantified by identifying LC3 puncta using CellProfiler and normalizing
1073 to the number of nuclei and the Mock DMSO control. Results were plotted in GraphPad and a 2-
1074 way ANOVA was performed with a Šidák's multiple comparison test, ±SEM n=5; *=P<0.05. B:
1075 HUVECs were infected as in A for 96 h and harvested in 2x Laemmli buffer. Protein lysates
1076 were resolved by SDS-PAGE and immunoblot was performed for phosphor-Beclin 1 (S90) and
1077 total Beclin 1. Samples were quantified using Image Lab (Biorad) software and then normalized,
1078 first to total protein and then to the Mock control. Results were plotted in GraphPad and a
1079 Student's t-test was performed, ±SEM n=3; *=P<0.05. C: HUVECs were infected with wild-
1080 type (WT) or delete KapB (delB) BAC16 KSHV via spinoculation and infection was allowed to

1081 proceed for 96 h prior to treatment with bafilomycin A1 (10 nM) for 30 min. Coverslips were
1082 fixed in methanol and immunostained for LC3 (autophagosomes; white) and DAPI (nuclei,
1083 blue). Cells were visually assessed for infection via LANA immunofluorescence. Scale bar=20
1084 µm. Total LC3 area per field was quantified by identifying LC3 puncta using CellProfiler and
1085 normalizing to the number of nuclei and the Mock DMSO control. Results were plotted in
1086 GraphPad and a 2-way ANOVA was performed with a Šidák's multiple comparison test, ±SEM
1087 n=3; *P<0.05. D: HUVECs were infected as in C for 96 h and harvested in 2x Laemmli buffer.
1088 Protein lysates were resolved by SDS-PAGE and immunoblot was performed for phospho-
1089 Beclin 1 (S90) and total Beclin 1. Samples were quantified using Image Lab (Biorad) software
1090 and then normalized, first to total protein and then to the Mock control. Results were plotted in
1091 GraphPad and a one-way ANOVA was performed, ±SEM n=3; *=P<0.05.

1092

1093 **Figure 7: KSHV-mediated PB disassembly requires Atg5 and the selective autophagy**
1094 **receptor NDP52.** A: HUVECs were transduced with recombinant lentivirus expressing shRNAs
1095 targeting Atg5, NDP52, or a non-targeting control (NS) and selected with puromycin (1 µg/mL).
1096 Cells were infected with rKSHV.219 via spinoculation and infection was allowed to proceed for
1097 96 h. Coverslips were fixed in 4% paraformaldehyde, permeabilized in 0.1% Triton X-100 and
1098 immunostained for Hedls (PBs; white), LANA (KSHV latency, green), and DAPI (nuclei, blue).
1099 Scale bar=20 µm. Hedls puncta were quantified using CellProfiler and presented as number of
1100 Hedls puncta per cell, all cells counted are displayed. Results were plotted in GraphPad and a 2-
1101 way ANOVA was performed on the main column effects with a Tukey's multiple comparison
1102 test, bar represents the mean; n=3, *=P<0.05. B: HUVECs were transduced with recombinant
1103 lentiviruses and infected with rKSHV.219 as in A. Cells were harvested in 2X Laemmli buffer.

1104 Protein lysates were resolved by SDS-PAGE and immunoblot was performed for Atg5 and
1105 NDP52. C. Model of PB disassembly induced by KSHV/KapB. KapB increases the
1106 phosphorylation of Beclin 1 at Serine 90 to enhance autophagic flux while Torin induces
1107 autophagic flux via the inhibition of mTORC1/2 and dephosphorylation of the ULK complex.
1108 Enhanced activation of autophagic flux by either mechanism results in PB disassembly that is
1109 dependent on the selective autophagy receptor, NDP52. In our model, we predict that NDP52
1110 recruits a PB component(s) to the nascent autophagosome. Our top candidate for this recruitment
1111 is Dcp1a, as steady state levels of Dcp1a decrease in response to KapB expression or Torin
1112 treatment, and Dcp1a is required for PB stability. Autophagic degradation of Dcp1a and/or
1113 another PB component leads to PB disassembly.
1114
1115
1116

1117 **Tables**

1118 Table 1: Drugs

Drug	Vendor/Catalogue #	Concentration
Torin1	Sigma-Aldrich 475991	250 nM
Bafilomycin A1	Sigma-Aldrich B1793	10 nM
Chloroquine	Sigma-Aldrich C6628	25 µM
MG-132	Selleckchem S2619	5 µM
LPS	Sigma-Aldrich L3129	1 µg/mL
Sodium Arsenite	Sigma-Aldrich 1.06277	0.25 mM
Doxycycline	Sigma-Aldrich D9891	1 µg/mL

1119

1120 Table 2: Plasmids

Plasmid	Use	Source	Mammalian Selection
RFP-NDP52	Overexpression	Dr. Andreas Till (University Hospital of Bonn)	N/A
pcDNA 3.1 (+)	Empty Vector Control	Invitrogen V79020	N/A
pcDNA KapB BCBL1	ARE-mRNA stability	(51)	N/A
pcDNA FLAG-MK2EE	ARE-mRNA stability	(51)	N/A
pLKO.1-TRC	shRNA expression	Addgene #10878 (122)	Puromycin
pLKO.1-blast	shRNA expression	Addgene #26655 (123)	Blasticidin
pLJM1	Empty Vector Control	(124)	Blasticidin/ Puromycin
pLJM1 KapB (pulmonary KS)	Overexpression	Cloned from pBMNIP-KapB (51) into pLJM1-BSD	Blasticidin
pLJM1 mCh	Overexpression Control	Craig McCormick (Dalhousie University)	Blasticidin
pLJM1 FLAG-MK2EE	Overexpression	Cloned into pLJM1 using BamHI and EcoRI from pBMN FLAG-MK2EE (51)	Blasticidin/ Puromycin
pLJM1 RFP-NDP52	Overexpression	Cloned into pLJM1 using NheI and BamHI from RFP-NDP52	Puromycin
pMD2.G	Lentivirus generation	Addgene #12259	N/A
psPAX2	Lentivirus generation	Addgene #12260	N/A
pTRE2 Firefly Luciferase-ARE	ARE-mRNA stability	(65)	N/A
pTRE2-Renilla Luciferase	ARE-mRNA stability	(65)	N/A

1121

1122 Table 3: shRNA target sequences

shRNA target	shRNA sequence 5'→3'	Region

Non-targeting (NS)	AGCACAAGCTGGAGTACAACTA	
Atg14	GTCTGGCAAATCTTCGACGAT	CDS
Atg5	CTTTGATAATGAACAGTGAGA	CDS
NDP52(1)	GAGCTGCTTCAACTGAAAGAA	CDS
NDP52(2)	GACTTGCCTATGGAAACCCAT	CDS
NDP52(3)	CCCTTTGTGAACTAAGTTCAA	3'-UTR
NDP52(4)	CCTGACTTGATACTAAGTGAT	3'-UTR
Optineurin (1)	GCACGGCATTGTCTAAATATA	CDS
Optineurin (2)	GCCATGAAGCTAAATAATCAA	CDS
p62	CCGAATCTACATTAAAGAGAA	CDS
NBR1 (1)	GCCAGGAACCAAGTTTATCAA	CDS
NBR1 (2)	CCATCCTACAATATCTGTGAA	CDS
VCP (1)	ACCGTCCCAATCGGTTAATTG	CDS
VCP (2)	AGATCCGTCGAGATCACTTTG	CDS

Table 4: Antibodies

Antibody	**Species**	**Vendor/Catalogue #**	**Application**	**Dilution**
Hedls	Mouse	Santa Cruz sc-8418	Immunofluorescence Immunoblot	1:1000 1:1000
KapB	Rabbit	A generous gift from Don Ganem	Immunofluorescence	1:1000
NDP52	Rabbit	CST 60732	Immunoblot	1:1000
p62	Rabbit	CST 7695	Immunoblot	1:1000
Dcp1a	Mouse	CST 15365	Immunoblot	1:500
DDX6	Rabbit	Bethyl A300-461	Immunoblot	1:1000
MK2	Rabbit	CST 12155	Immunofluorescence	1:1000
LC3B	Rabbit	CST 2775	Immunofluorescence Immunoblot	1:200 1:1000
Atg5	Rabbit	CST 2630	Immunoblot	1:1000
Atg14	Rabbit	CST 96752	Immunoblot	1:1000
OPTN	Rabbit	Abcam ab23666	Immunoblot	1:1000
Xrn1	Rabbit	Abcam ab231197	Immunoblot	1:1000
VCP	Rabbit	CST 2649	Immunoblot	1:1000
NBR1	Rabbit	CST 9891	Immunoblot	1:1000
LANA	Rabbit	A generous gift from Don Ganem	Immunofluorescence	1:1000
Phospho-S6 (Ser235/236)	Rabbit	CST 4858	Immunoblot	1:1000
Total S6	Rabbit	CST 2217	Immunoblot	1:1000
Phospho-Beclin 1 (Ser90)	Rabbit	CST 86455	Immunoblot	1:500
Total Beclin 1	Mouse	CST 4122	Immunoblot	1:1000
Phospho-ULK (Ser555)	Rabbit	CST 5869	Immunoblot	1:1000

Phospho-ULK (Ser757)	Rabbit	CST 14202	Immunoblot	1:1000
Total ULK	Rabbit	CST 8054	Immunoblot	1:1000

1125

1126 Table 5: qPCR primers

Primer	**Primer Sequence**
HPRT-1- Forward	5' CTTTCCTTGGTCAGGCAGTATAA 3'
HPRT-1 - Reverse	5' AGTCTGGCTTATATCCAACACTTC 3'
18S - Forward	5' TTCGAACGTCTGCCCTATCAA 3'
18S - Reverse	5' GATGTGGTAGCCGTTTCTCAGG 3'
IL-6 - Forward	5' GAAGCTCTATCTCGCCTCCA 3'
IL-6 - Reverse	5' TTTTCTGCCAGTGCCTCTTT 3'
CXCL8 - Forward	5' AAATCTGGCAACCCTAGTCTG 3'
CXCL8 - Reverse	5' GTGAGGTAAGATGGTGGCTAAT 3'
IL-1β - Forward	5' CTCTCACCTCTCCTACTCACTT 3'
IL-1β - Reverse	5' TCAGAATGTGGGAGCGAATG 3'
COX-2 - Forward	5' CCCTTGGGTGTCAAAGGTAA 3'
COX-2 - Reverse	5' GCCCTCGCTTATGATCTGTC 3'

1127

1128 **<u>Supplemental Figure Legends</u>**

1129 **Figure S1: KapB expression promotes PB disassembly but does not prevent PB assembly.**

1130 HeLa cells expressing a doxycycline-inducible GFP-Dcp1a were used to determine whether

1131 KapB prevented granule assembly or promoted disassembly. A: HeLa cells were transfected with

1132 either KapB or an empty vector control prior to inducing expression of GFP-Dcp1a with

1133 doxycycline (1 µg/mL). Cells were fixed 12 h post-induction and immunostained for Hedls (PBs,

1134 red) and KapB (blue). Scale bar=20 µm. B: GFP-Dcp1a expression was induced with

1135 doxycycline (1 µg/mL) in HeLa cells prior to transfection with either KapB or an empty vector

1136 control. Cells were fixed 12 h post-transfection and immunostained for Hedls (PBs, red) and

1137 KapB (blue). Scale bar=20 µm. C: HUVECs were transduced with recombinant lentiviruses

1138 expressing either Kaposin B (KapB) or an empty vector control and selected with blasticidin (5

1139 µg/mL). Cells were treated with sodium arsenite (0.25 mM) or a vehicle control for 30 min prior

1140 to fixation in 4% paraformaldehyde and permeabilization in 0.1% Triton X-100. Scale bar=20

1141 µm.

1142 **Figure S2: Canonical autophagy knockdown prevents KapB-mediated PB disassembly.**
1143 A&B: HUVECs were sequentially transduced: first with recombinant lentiviruses expressing
1144 either shRNAs targeting Atg5 or Atg14 (shAtg5, shAtg14) or a non-targeting control (NS) and
1145 selected with puromycin (1 µg/mL), and second with either KapB or an empty vector control and
1146 selected with blasticidin (5 µg/mL). Samples were lysed in 2x Laemmli and resolved by SDS-
1147 PAGE. Samples were immunoblotted for Atg5 (A) or Atg14 (B). For Atg5 (A), representative
1148 blot is from the same membrane, hashed line indicates skipped lanes. For Atg5 (A) samples were
1149 quantified by normalizing Atg5 protein levels to the total protein in each lane using Image Lab
1150 (Biorad) and then to Vector NS. Results were plotted in GraphPad, a 2-way ANOVA was
1151 performed, ±SEM; n=3, ***=P<0.001. C: Atg5 +/+ (WT) and -/- (KO) MEFs were transduced as
1152 in A and harvested in 2x Laemmli buffer before being resolved by SDS-PAGE. Samples were
1153 probed for LC3, a representative blot is shown. D: Atg5 +/+ and -/- MEFs were transduced with
1154 recombinant viruses expressing KapB or an empty vector control and selected with blasticidin (5
1155 µg/mL). Samples were fixed in 4% paraformaldehyde and permeabilized in 0.1% Triton X-100.
1156 Immunofluorescence was performed for Hedls (PBs, white) and DAPI (nuclei, blue). Scale
1157 bar=20 µm. Hedls puncta were quantified using CellProfiler and presented as number of Hedls
1158 puncta per cell, all cells counted are displayed. Results were plotted in GraphPad and a 2-way
1159 ANOVA was performed on the main column effects with a Tukey's multiple comparison test,
1160 bar represents the mean; n=3, **=P<0.01.
1161
1162 **Figure S3: Canonical autophagy shRNA silencing in HeLa cells.** A&B: HeLas were
1163 transduced with recombinant lentiviruses expressing either shRNAs targeting Atg5 or Atg14
1164 (shAtg5, shAtg14) or a non-targeting control (NS) and selected with puromycin (1 µg/mL) prior

1165 to transfection with KapB or an empty vector for luciferase assays. Samples were lysed in 2x
1166 Laemmli buffer and resolved by SDS-PAGE before immunoblotting with Atg5 (A) or Atg14 (B).
1167 Representative blots are shown.
1168
1169 **Figure S4: Selective autophagy receptor knockdown in HUVECs reveals that OPTN and**
1170 **p62 are not required for KapB-mediated PB disassembly.** A&B: HUVECs were transduced
1171 with shRNAs targeting VCP, NBR1, or a non-targeting control (NS) and selected with
1172 puromycin (1 µg/mL), then transduced with an empty vector control or KapB and selected with
1173 blasticidin (5 µg/mL). Samples were lysed in 2x Laemmli buffer, resolved by SDS-PAGE, and
1174 immunoblotted for NBR1 (A) and VCP (B). Representative blots are shown, successful VCP
1175 knockdown was lethal, while NBR1 knockdown was not successful. C: HUVECs were
1176 transduced with shRNAs targeting NDP52 or a non-targeting control (NS) and selected with
1177 puromycin (1 µg/mL), then transduced with an empty vector control or KapB and selected with
1178 blasticidin (5 µg/mL). Samples were lysed in 2x Laemmli buffer, resolved by SDS-PAGE, and
1179 immunoblotted for NDP52. D&E: HUVECs were transduced with shRNAs targeting p62,
1180 OPTN, or a non-targeting control (NS) and selected with puromycin (1 µg/mL), then transduced
1181 with an empty vector control or KapB and selected with blasticidin (5 µg/mL). Samples were
1182 lysed in 2x Laemmli buffer and resolved by SDS-PAGE. Samples were immunoblotted for p62
1183 (D) and OPTN (E), representative blots are shown. F: HUVECs were transduced as in D and E.
1184 Coverslips were fixed in 4% paraformaldehyde, permeabilized in 0.1% Triton X-100 and
1185 immunostained for Hedls (PBs; white), DAPI (nuclei, blue). Scale bar=20 µm. Hedls puncta
1186 were quantified using CellProfiler and presented as number of Hedls puncta per cell, all cells
1187 counted are displayed. Results were plotted in GraphPad and a 2-way ANOVA was performed

1188 on the main column effects with a Tukey's multiple comparison test, bar represents the mean;
1189 n=3, **=P<0.01. G: HUVECs were transduced with recombinant lentiviruses targeting NDP52
1190 or a non-targeting control (NS) and selected with puromycin (1 µg/mL). Samples were lysed in
1191 2x Laemmli buffer, resolved by SDS-PAGE, and immunoblotted for NDP52 to confirm
1192 knockdown for paired Torin immunofluorescence experiments.
1193
1194 **Figure S5: shRNA silencing of selective autophagy receptors in HeLa cells.** A, B&C: HeLas
1195 were transduced with shRNAs targeting NDP52, OPTN, p62, or a non-targeting control (NS) and
1196 selected with puromycin (1 µg/mL) prior to transfection with KapB or an empty vector for
1197 luciferase assays. Samples were lysed in 2x Laemmli buffer, resolved by SDS-PAGE, and
1198 immunoblotted for NDP52 (A), p62 (B), and OPTN (C). Representative blots are shown.
1199
1200 **Figure S6: NDP52 shRNA silencing and rescue in control HUVECs.** A: Representative
1201 western blot of HUVECs transduced with an shRNA targeting the 3'UTR of NDP52 or a non-
1202 targeting control (NS) and selected with puromycin (1 µg/mL), then co-transduced with an
1203 empty vector control and mCherry (mCh) or KapB and mCh. Samples were lysed in 2x
1204 Laemmli, resolved by SDS-PAGE, and immunoblotted for NDP52. B: HUVECs were
1205 sequentially transduced first with recombinant lentivirus expressing shDNP52 targeting the 3'-
1206 UTR of NDP52 or a NS control and selected with blasticidin (5 µg/mL), and second, with vector
1207 and either an mCherry control (mCh) or RFP-NDP52. Coverslips were fixed with 4% v/v
1208 paraformaldehyde, permeabilized with 0.1% Triton X-100, and were immunostained with Hedls
1209 (PBs, green). Scale bar=20 µm. C: Hedls puncta were quantified using CellProfiler and presented
1210 as number of Hedls puncta per cell, all cells counted are displayed. Results were plotted in

1211 GraphPad and a 2-way ANOVA was performed on the main column effects with a Tukey's

1212 multiple comparison test, bar represents the mean; n=3.

1213

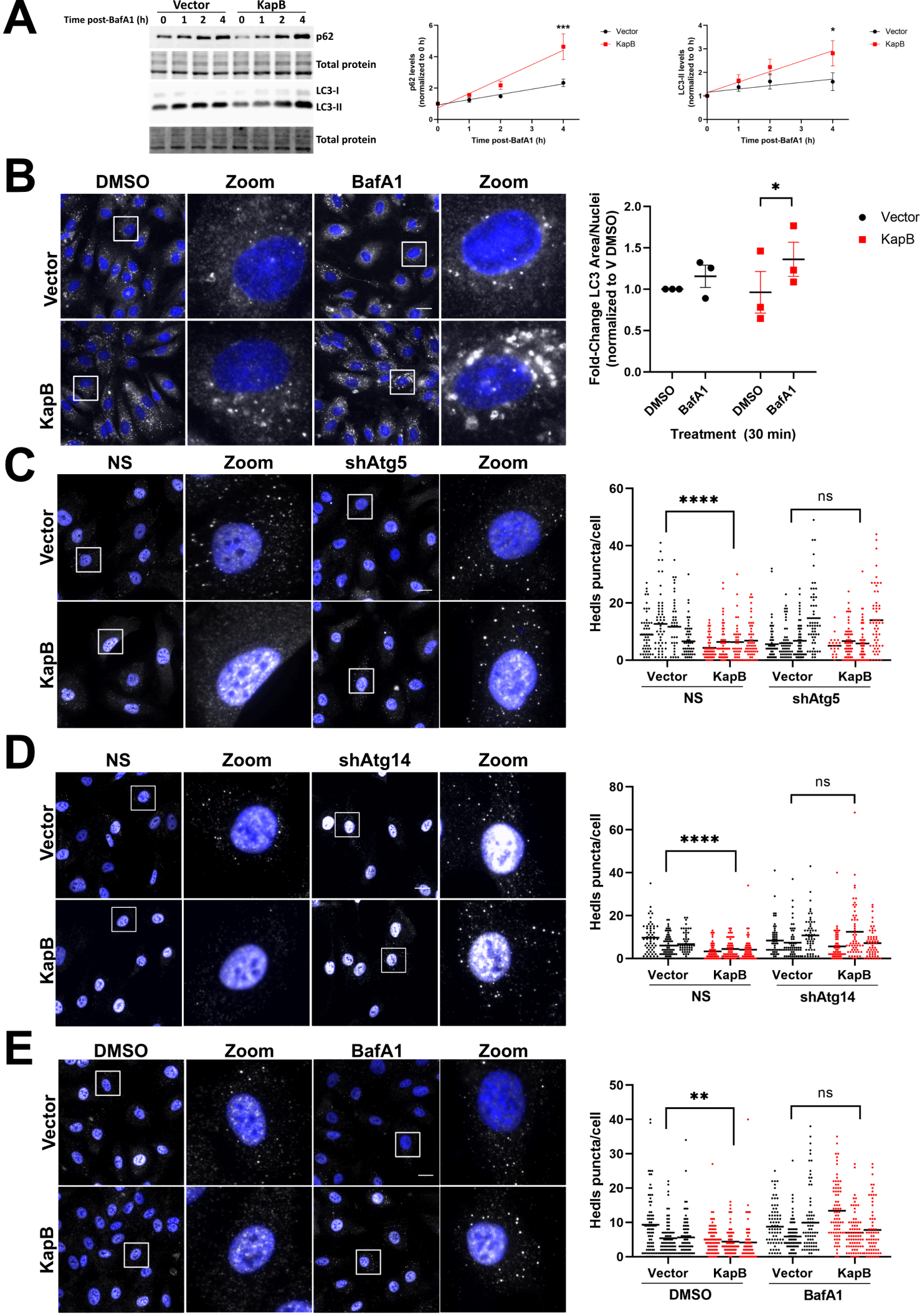
A
Vector
KapB
Time post-BafA1 (h)
0 1 2 4 0 1 2 4
p62
Total protein
LC3-I
LC3-II
Total protein
p62 levels (normalized to 0 h)
Time post-BafA1 (h)
***
Vector
KapB
LC3-II levels (normalized to 0 h)
Time post-BafA1 (h)
*
Vector
KapB
B
DMSO
Zoom
BafA1
Zoom
Vector
KapB
Fold-Change LC3 Area/Nuclei (normalized to V DMSO)
*
Vector
KapB
DMSO
BafA1
DMSO
BafA1
Treatment (30 min)
C
NS
Zoom
shAtg5
Zoom
Vector
KapB
Hedls puncta/cell
****
ns
Vector
KapB
Vector
KapB
NS
shAtg5
D
NS
Zoom
shAtg14
Zoom
Vector
KapB
Hedls puncta/cell
****
ns
Vector
KapB
Vector
KapB
NS
shAtg14
E
DMSO
Zoom
BafA1
Zoom
Vector
KapB
Hedls puncta/cell
**
ns
Vector
KapB
Vector
KapB
DMSO
BafA1

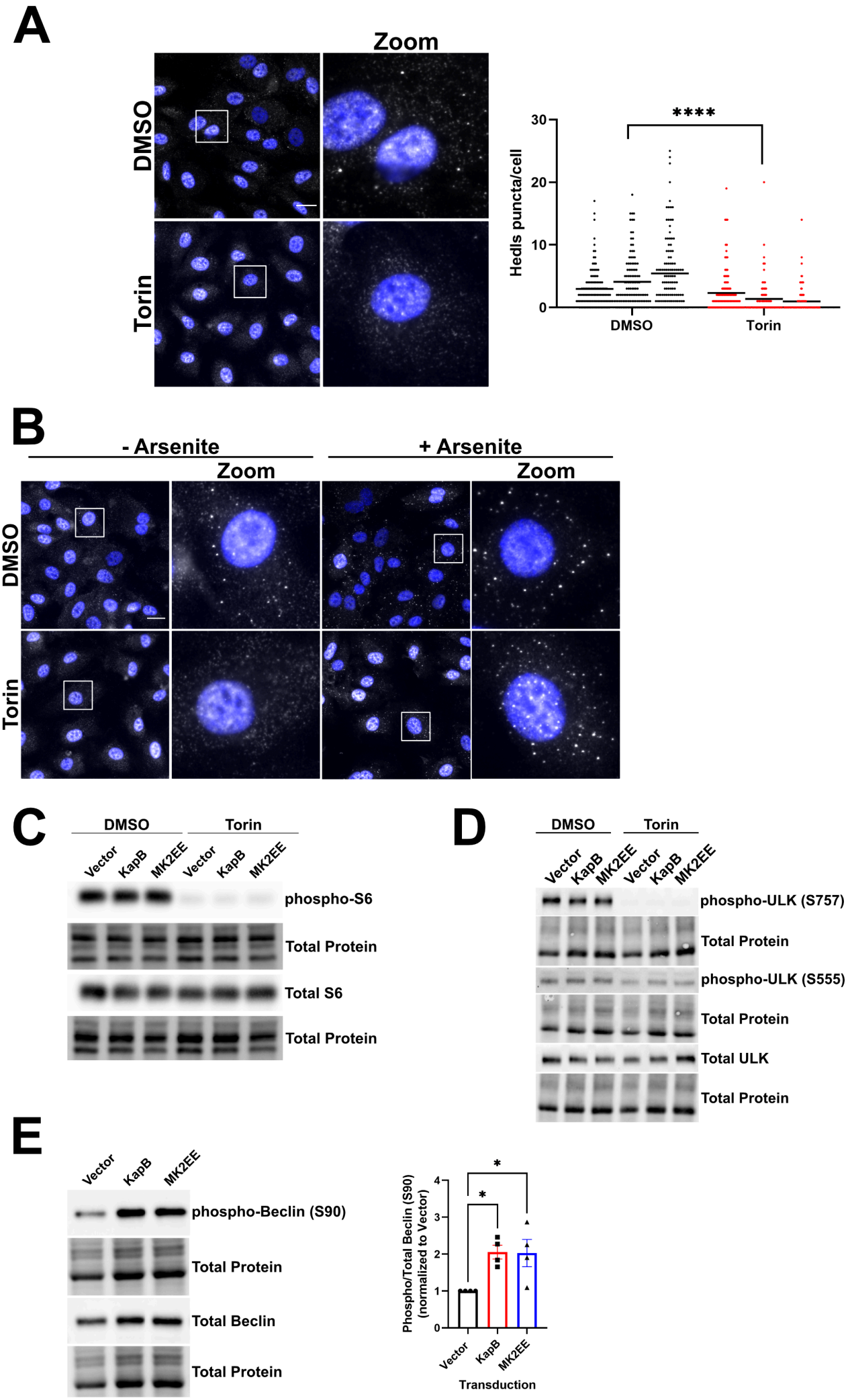
A
Zoom
DMSO
Torin
****
Hedls puncta/cell
30
20
10
0
DMSO
Torin
B
- Arsenite
+ Arsenite
Zoom
Zoom
DMSO
Torin
C
DMSO
Torin
Vector
KapB
MK2EE
Vector
KapB
MK2EE
phospho-S6
Total Protein
Total S6
Total Protein
D
DMSO
Torin
Vector
KapB
MK2EE
Vector
KapB
MK2EE
phospho-ULK (S757)
Total Protein
phospho-ULK (S555)
Total Protein
Total ULK
Total Protein
E
Vector
KapB
MK2EE
phospho-Beclin (S90)
Total Protein
Total Beclin
Total Protein
*
*
Phospho/Total Beclin (S90)
(normalized to Vector)
4
3
2
1
0
Vector
KapB
MK2EE
Transduction

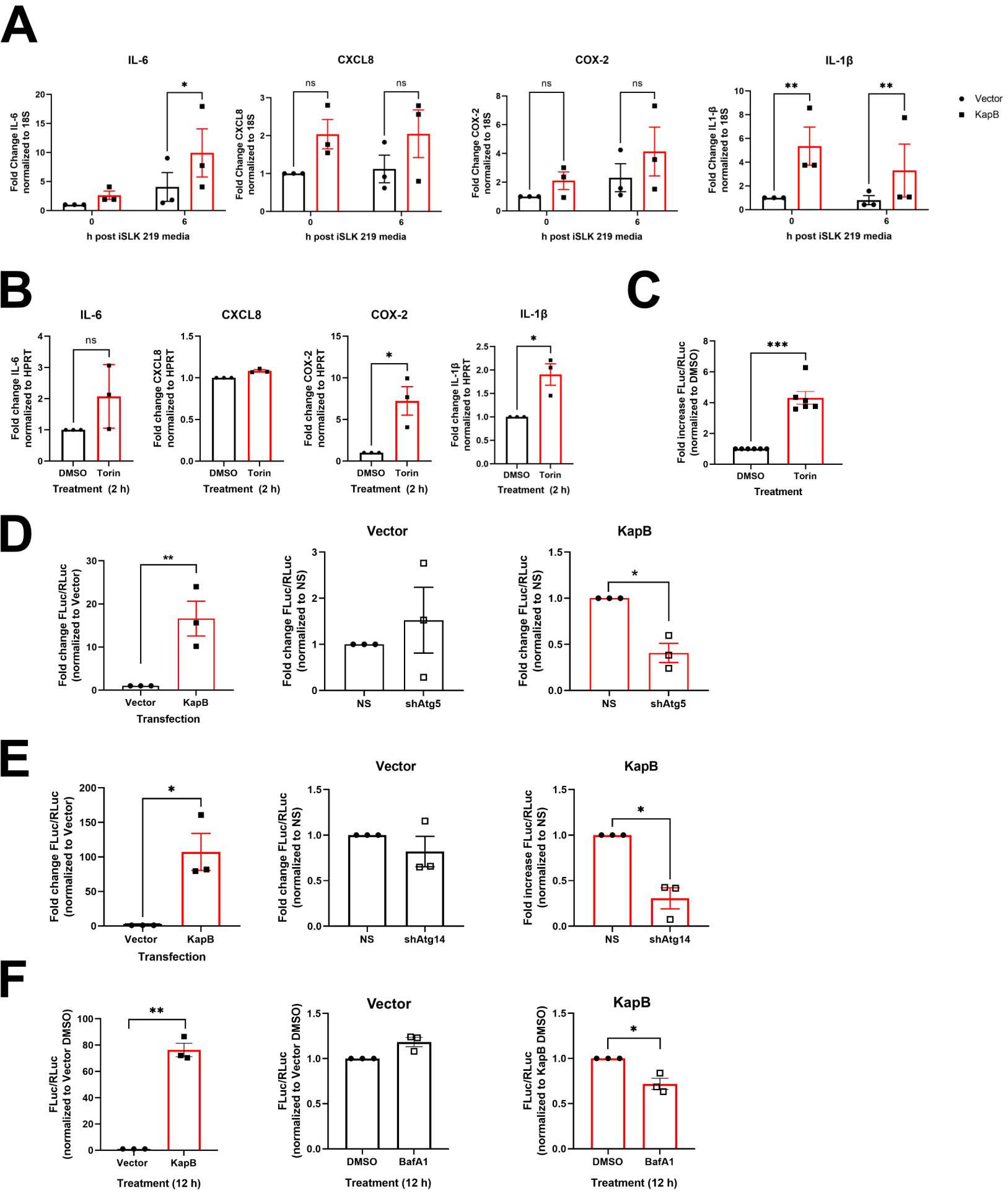
A
IL-6
CXCL8
COX-2
IL-1β
Fold Change IL-6 normalized to 18S
Fold Change CXCL8 normalized to 18S
Fold Change COX-2 normalized to 18S
Fold Change IL1-β normalized to 18S
h post iSLK 219 media
Vector
KapB
B
Fold change IL-6 normalized to HPRT
Fold change CXCL8 normalized to HPRT
Fold change COX-2 normalized to HPRT
Fold change IL-1β normalized to HPRT
DMSO
Torin
Treatment (2 h)
C
Fold increase FLuc/RLuc (normalized to DMSO)
Treatment
D
Fold change FLuc/RLuc (normalized to Vector)
Transfection
Fold change FLuc/RLuc (normalized to NS)
NS
shAtg5
E
Fold increase FLuc/RLuc (normalized to NS)
shAtg14
F
FLuc/RLuc (normalized to Vector DMSO)
FLuc/RLuc (normalized to Vector DMSO)
FLuc/RLuc (normalized to KapB DMSO)
BafA1
Treatment (12 h)

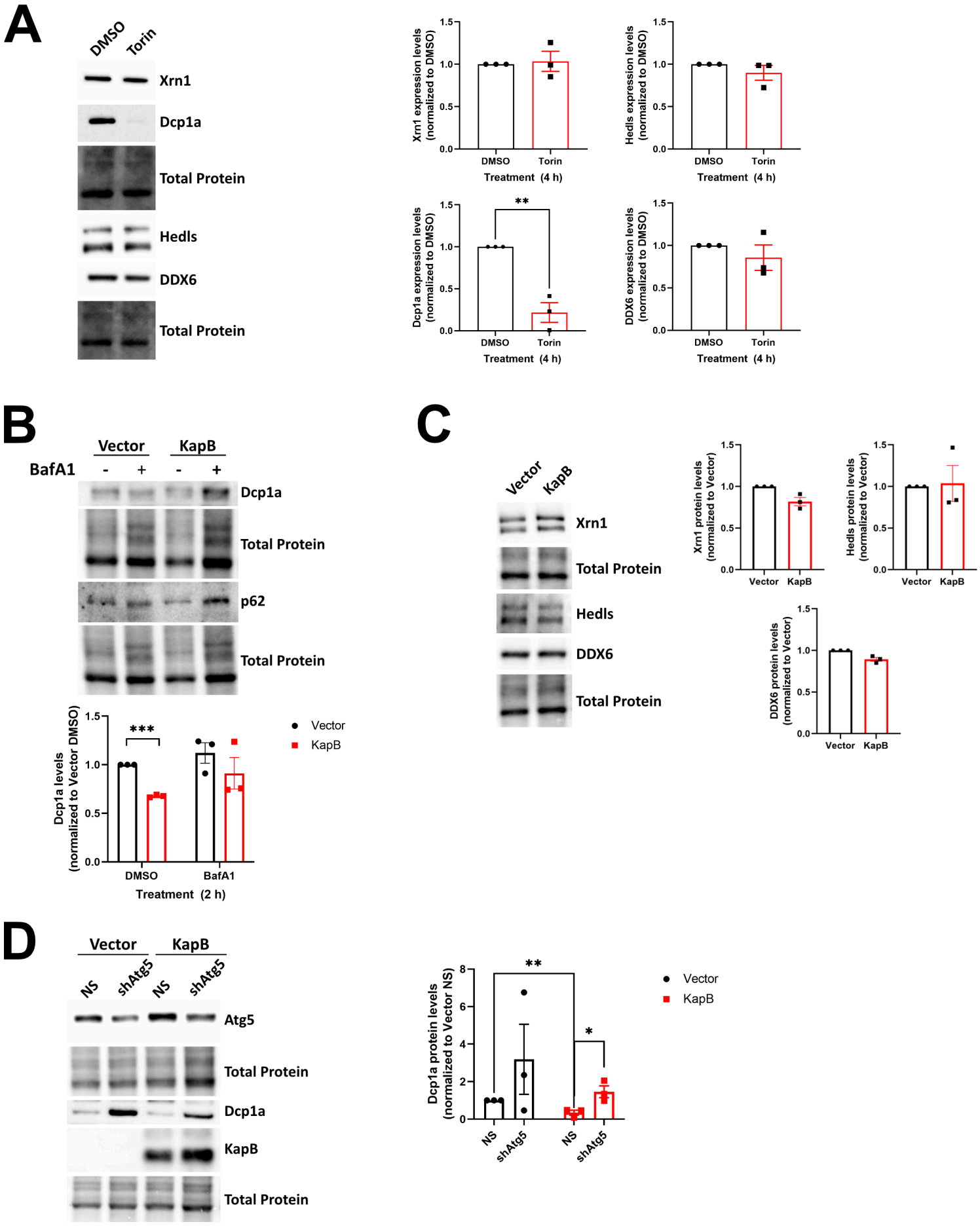
A
DMSO
Torin
Xrn1
Dcp1a
Total Protein
Hedls
DDX6
Total Protein
Xrn1 expression levels (normalized to DMSO)
Hedls expression levels (normalized to DMSO)
Dcp1a expression levels (normalized to DMSO)
DDX6 expression levels (normalized to DMSO)
1.5
1.0
0.5
0.0
**
DMSO
Torin
Treatment (4 h)
B
Vector
KapB
BafA1
-
+
-
+
Dcp1a
Total Protein
p62
Total Protein
Dcp1a levels (normalized to Vector DMSO)
***
Vector
KapB
DMSO
BafA1
Treatment (2 h)
C
Vector
KapB
Xrn1
Total Protein
Hedls
DDX6
Total Protein
Xrn1 protein levels (normalized to Vector)
Hedls protein levels (normalized to Vector)
DDX6 protein levels (normalized to Vector)
Vector
KapB
D
Vector
KapB
NS
shAtg5
NS
shAtg5
Atg5
Total Protein
Dcp1a
KapB
Total Protein
Dcp1a protein levels (normalized to Vector NS)
8
6
4
2
0
**
*
Vector
KapB
NS
shAtg5
NS
shAtg5

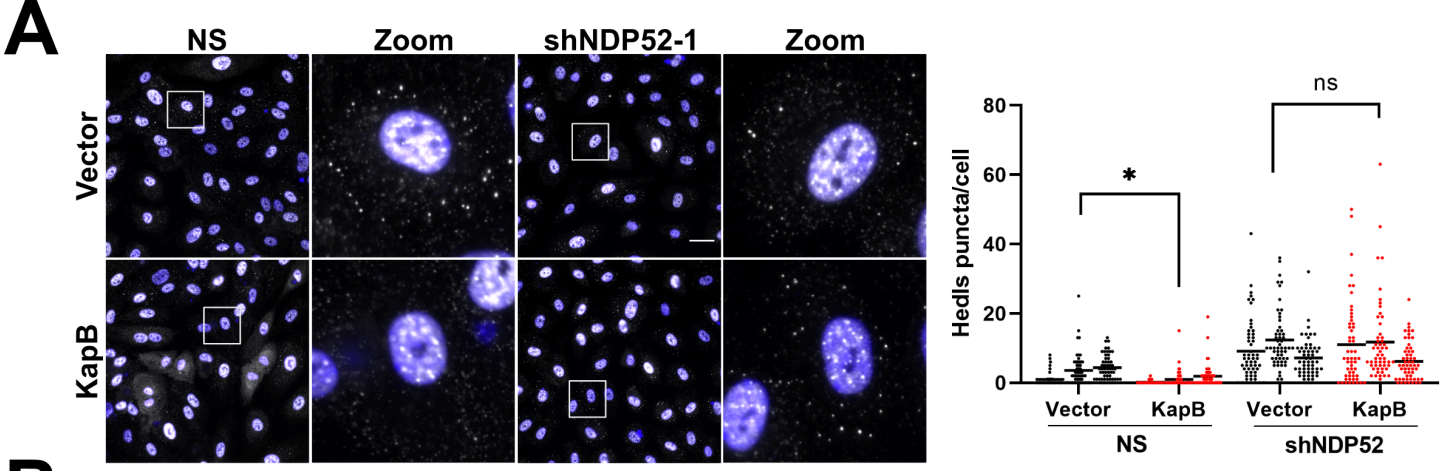
A
NS
Zoom
shNDP52-1
Zoom
Vector
KapB
Hedls puncta/cell
80
60
40
20
0
*
ns
Vector
KapB
Vector
KapB
NS
shNDP52

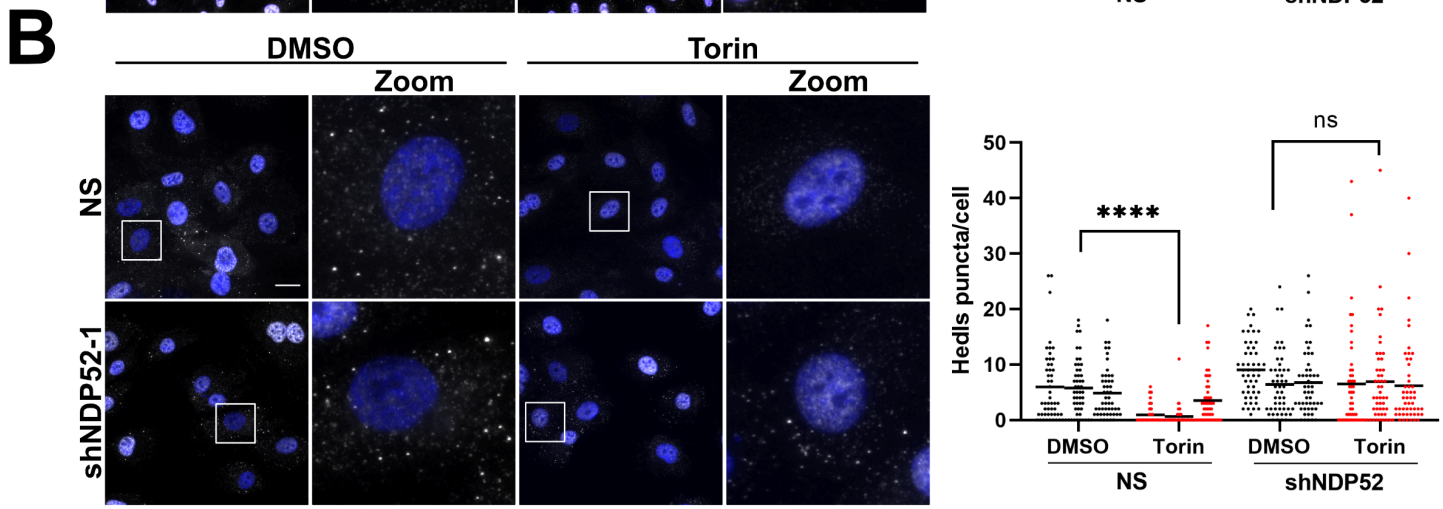
B
DMSO
Torin
Zoom
Zoom
NS
shNDP52-1
Hedls puncta/cell
50
40
30
20
10
0
****
ns
DMSO
Torin
DMSO
Torin
NS
shNDP52

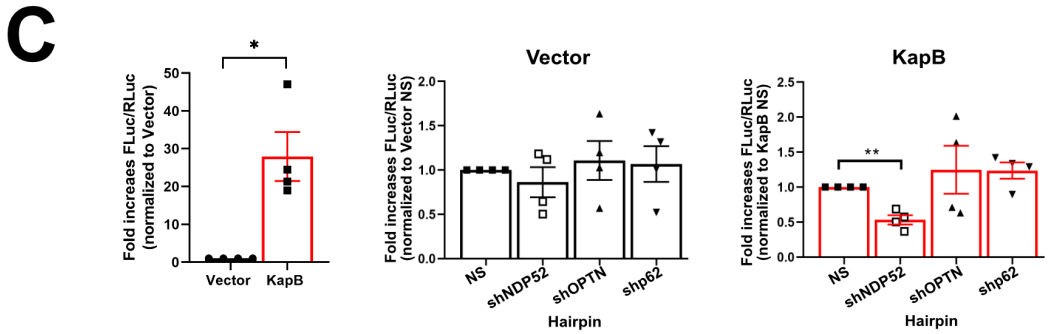
C
Fold increaes FLuc/RLuc (normalized to Vector)
*
Vector
KapB
Vector
Fold increases FLuc/RLuc (normalized to Vector NS)
NS
shNDP52
shOPTN
shp62
Hairpin
KapB
Fold increases FLuc/RLuc (normalized to KapB NS)
**
NS
shNDP52
shOPTN
shp62
Hairpin

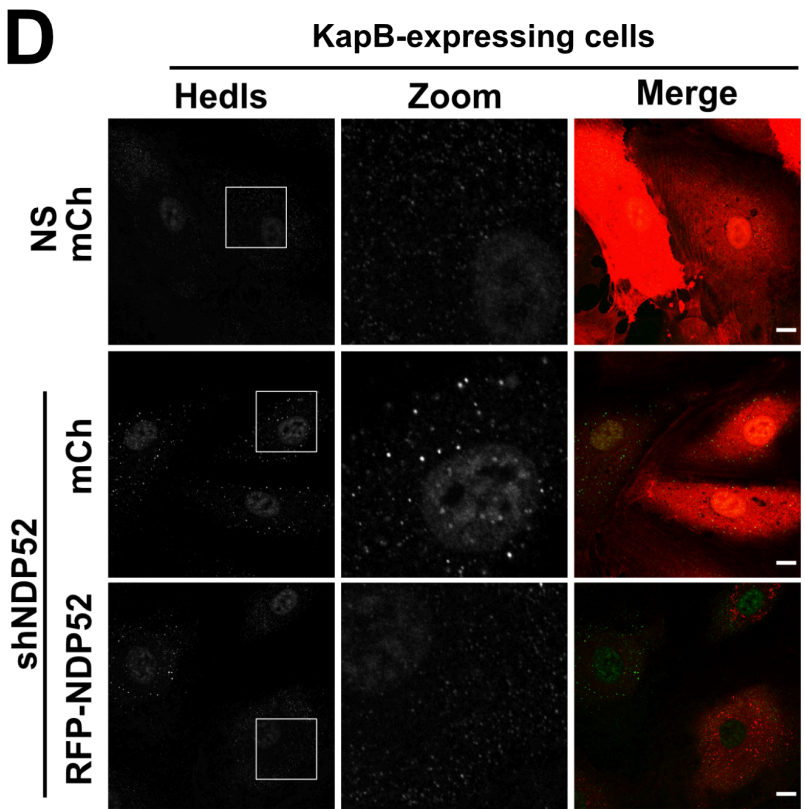
D
KapB-expressing cells
Hedls
Zoom
Merge
NS mCh
shNDP52
mCh
RFP-NDP52

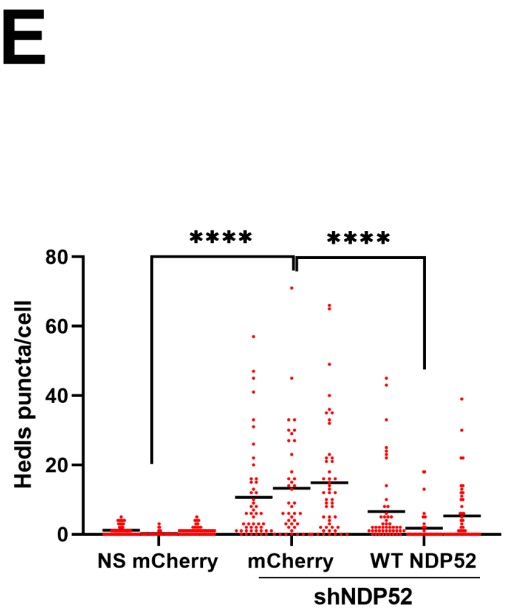
E
Hedls puncta/cell
80
60
40
20
0
****
****
NS mCherry
mCherry
WT NDP52
shNDP52

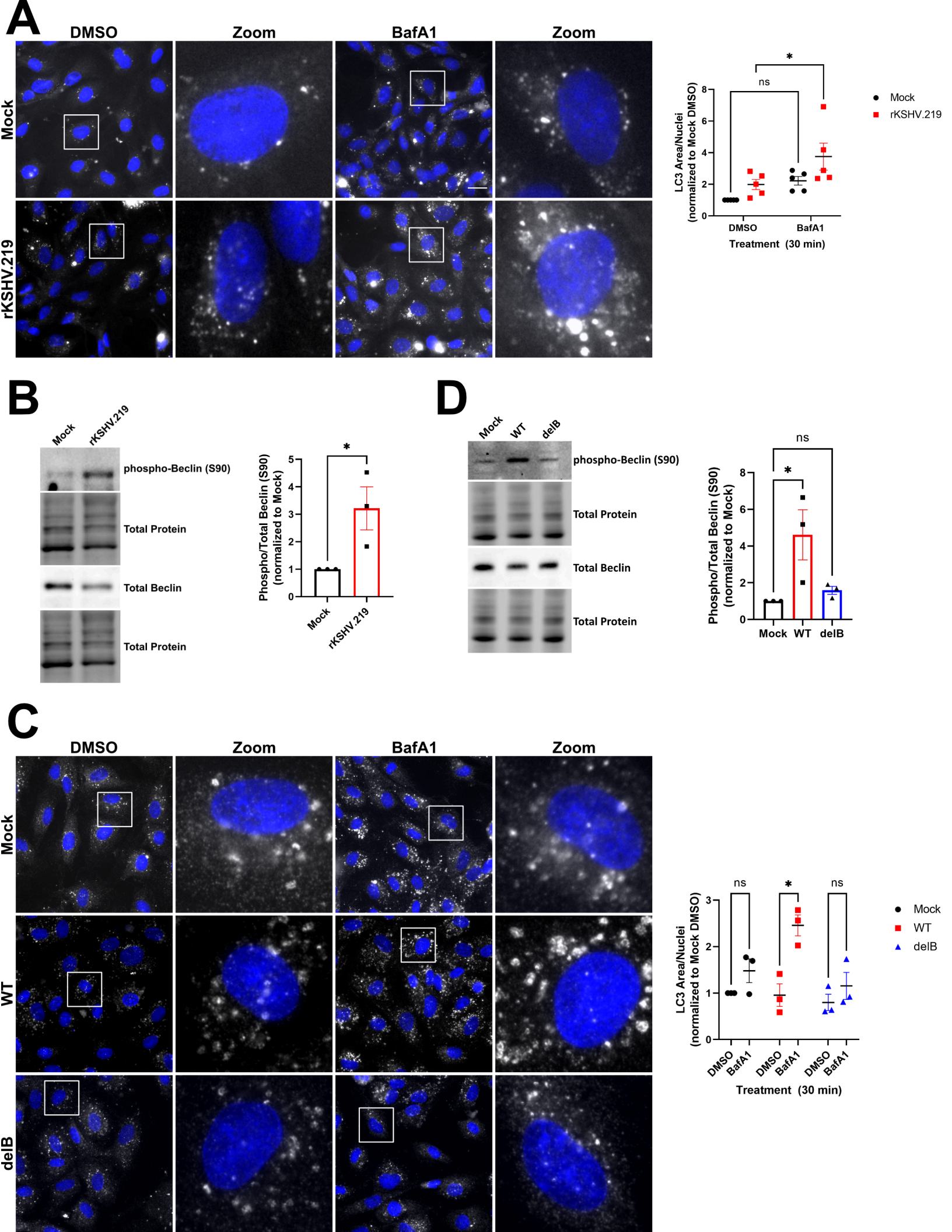
A
DMSO
Zoom
BafA1
Zoom
Mock
rKSHV.219
LC3 Area/Nuclei (normalized to Mock DMSO)
ns
*
Mock
rKSHV.219
DMSO
BafA1
Treatment (30 min)
B
Mock
rKSHV.219
phospho-Beclin (S90)
Total Protein
Total Beclin
Total Protein
Phospho/Total Beclin (S90) (normalized to Mock)
*
Mock
rKSHV.219
D
Mock
WT
delB
phospho-Beclin (S90)
Total Protein
Total Beclin
Total Protein
Phospho/Total Beclin (S90) (normalized to Mock)
ns
*
Mock
WT
delB
C
DMSO
Zoom
BafA1
Zoom
Mock
WT
delB
LC3 Area/Nuclei (normalized to Mock DMSO)
ns
*
ns
Mock
WT
delB
DMSO
BafA1
DMSO
BafA1
DMSO
BafA1
Treatment (30 min)

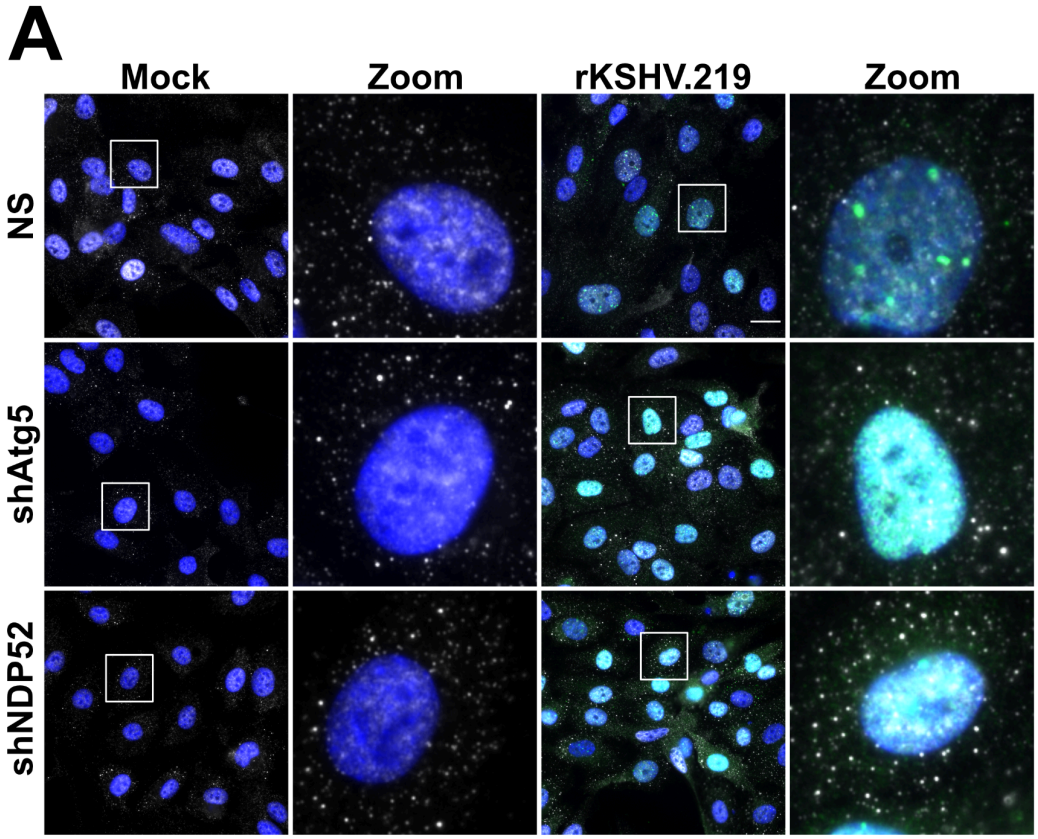
A
Mock
Zoom
rKSHV.219
Zoom
NS
shAtg5
shNDP52

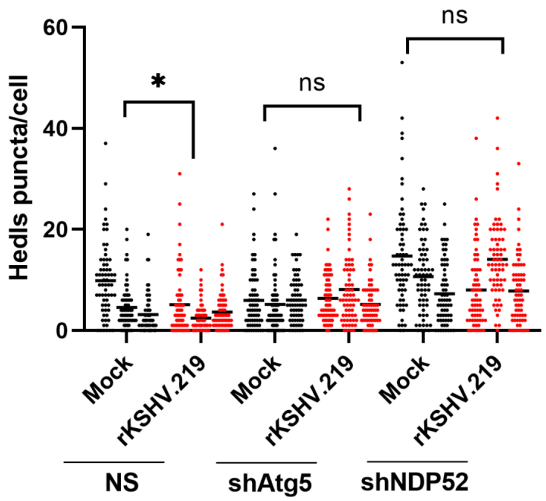
Hedls puncta/cell
60
40
20
0
*
ns
ns
Mock
rKSHV.219
Mock
rKSHV.219
Mock
rKSHV.219
NS
shAtg5
shNDP52

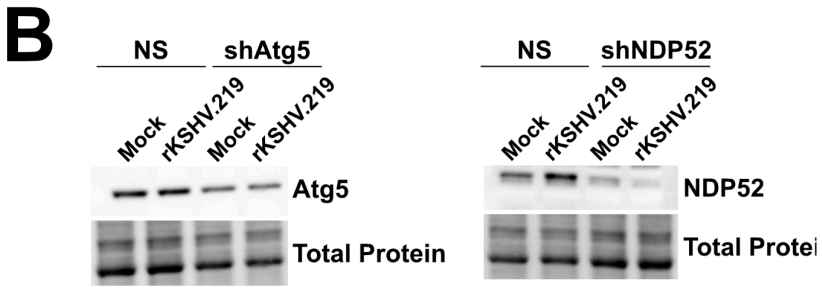
B
NS
shAtg5
Mock
rKSHV.219
Mock
rKSHV.219
Atg5
Total Protein
NS
shNDP52
Mock
rKSHV.219
Mock
rKSHV.219
NDP52
Total Protei

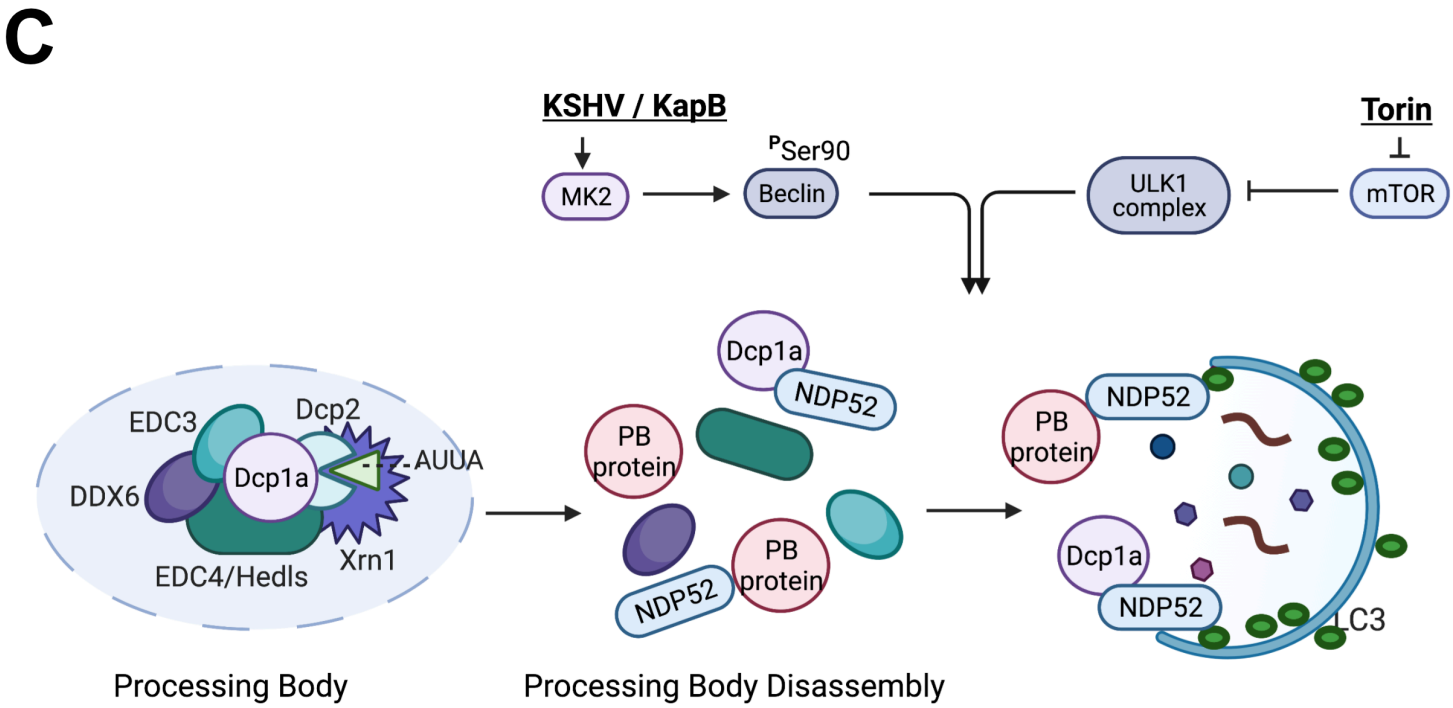
C
KSHV / KapB
MK2
PSer90
Beclin
ULK1 complex
Torin
mTOR
EDC3
Dcp2
Dcp1a
AUUA
DDX6
EDC4/Hedls
Xrn1
Processing Body
Dcp1a
NDP52
PB protein
NDP52
PB protein
Processing Body Disassembly
PB protein
NDP52
Dcp1a
NDP52
LC3